

THESIS FOR THE DEGREE OF DOCTOR OF PHILOSOPHY

Sodium Batteries: From Liquid to Polymer Electrolytes

ANDREA BOSCHIN



CHALMERS

Department of Physics

CHALMERS UNIVERSITY OF TECHNOLOGY

Göteborg, Sweden 2016

Sodium Batteries: From Liquid to Polymer Electrolytes

ANDREA BOSCHIN

Göteborg, 2016

ISBN 978-91-7597-517-7

© ANDREA BOSCHIN, 2016.

Doktorsavhandlingar vid Chalmers tekniska högskola

Ny serie nr: 4198

ISSN 0346-718X

Department of Physics

Chalmers University of Technology

SE-412 96 Göteborg, Sweden

Cover: Schematic of a sodium battery based on a liquid or polymer electrolyte.

Printed by Chalmers Reproservice

Göteborg, Sweden 2016

Sodium Batteries: From Liquid to Polymer Electrolytes

Andrea Boschin

Department of Physics

Chalmers University of Technology

SE-412 96 Göteborg, Sweden

Abstract

Today lithium-ion batteries (LIBs) are dominating the field of rechargeable batteries for portable devices. More recently LIBs have also been considered for large-scale applications, such as in the areas of electromobility and grid storage. With the growing demand of lithium and its limited resources/production and price issues, it is advantageous to also consider other chemistries to complement/replace LIBs. Sodium, being abundant and similar to lithium, is a suitable alternative. In addition, batteries also need to meet stringent safety requirements. These requirements will influence the selection of suitable battery components (electrodes, electrolyte, *etc.*) with the overall aim to obtain more sustainable and safer battery, while guaranteeing adequate performance.

The common electrolyte used in LIBs as well as the analogous sodium-ion batteries (SIBs) contains fluorinated salts dissolved in organic liquid solvents, with many intrinsic safety concerns. Appealing alternatives could be liquid electrolytes free of fluorine and organic liquids, or altogether solid electrolytes.

In this thesis, an overview of liquid and solid electrolytes for sodium (-ion) batteries is given, outlining their differences. Aiming at safer batteries, mainly two broad classes of electrolytes are studied: fluorine-free electrolytes and solid polymer electrolytes. A known drawback of the latter is the low ionic conductivity at room temperature, which can be improved by *e.g.* adding an ionic liquid, a salt which is liquid at room temperature. All electrolytes are evaluated in terms of their ionic conductivities, ionic speciation and, for the polymer electrolytes, polymer dynamics and stability *vs.* sodium metal.

Keywords: sodium batteries, liquid electrolytes, polymer electrolytes, electrochemical solid state cells

List of Publications

- I. “*Non-aqueous electrolytes for sodium-ion batteries*”, Alexandre Ponrouch, Damien Monti, Andrea Boschin, Bengt Steen, Patrik Johansson and M. Rosa Palacín, *Journal of Materials Chemistry A*, 3 (2015) 22-42
- II. “*Fluorine-free salts for aqueous lithium-ion and sodium-ion battery electrolytes*”, Elham Hosseini-Bab-Anari, Andrea Boschin, Toshihiko Mandai, Hyuma Masu, Kasper Moth-Poulsen and Patrik Johansson, *RSC Advances*, 6 (2016) 85194-85201
- III. “*Characterization of NaX (X: TFSI, FSI) – PEO based solid polymer electrolytes for sodium batteries*”, Andrea Boschin and Patrik Johansson, *Electrochimica Acta*, 175 (2015) 124-133
- IV. “*On the feasibility of sodium metal as pseudo-reference electrode in solid state electrochemical cells*”, Andrea Boschin, Muhammad E. Abdelhamid and Patrik Johansson, In manuscript
- V. “*Plasticization of NaX–PEO polymer electrolytes by Pyr₁₃X ionic liquids*”, Andrea Boschin and Patrik Johansson, *Electrochimica Acta*, 211 (2016) 1006-1015

Contribution Report

- I.** I performed the literature search for the polymer electrolytes and wrote the first draft of that section. I co-authored the rest of the paper.
- II.** I prepared the electrolytes and performed: part of the solubility tests, thermal analysis, IR and Raman analysis, ionic conductivity and the electrochemical stability windows experiments. I wrote the first draft about the above mentioned topics and I shared the first co-authorship together with Elham Hosseini-Bab-Anari.
- III.** I prepared all samples, performed all measurements, and analyzed all data. I wrote the first draft and was the main author of the manuscript.
- IV.** I initiated the idea, prepared all samples, performed all measurements, and analyzed all data. I wrote the first draft and was the main author of the manuscript.
- V.** I initiated the idea, prepared all samples, performed all measurements, and analyzed all data. I wrote the first draft and was the main author of the manuscript.

List of Acronyms

Al	Aluminium
BF_4^-	Tetrafluoroborate
ClO_4^-	Perchlorate
BMI	1-butyl-3-methyl-imidazolium
CE	Counter electrode
Cl^-	Chloride
CV	Cyclic Voltammetry
DEC	Diethyl carbonate
DMC	Dimethyl carbonate
DSC	Differential scanning calorimetry
DS	Dielectric spectroscopy
EC	Ethylene carbonate
EIS	Electrochemical impedance spectroscopy
EMC	Ethyl methyl carbonate
EMIm	1-ethyl-3-methyl-imidazolium
ESW	Electrochemical stability window
F^-	Fluoride
FSI	Bis(fluorosulfonyl)imide
GPE	Gel polymer electrolyte
HC	Hard carbon
IL	Ionic liquid
LFP	LiFePO_4
Li	Lithium
LIB	Lithium-ion battery
MM4411	(di-methyl ammonio)bis(butane-1-sulfonate)
Na	Sodium
NASICON	Na Super Ionic CONductor
NiMH	Nickel-metal hydride
NO_3^-	Nitrate
NVP	$\text{Na}_3\text{V}_2(\text{PO}_4)_3$
NVPF	$\text{Na}_3\text{V}_2(\text{PO}_4)_2\text{F}_3$
PC	Propylene carbonate
PEO	Poly(ethylene oxide)
PF_6^-	hexafluorophosphate
Pyr_{13}	N-propyl-N-methyl-pyrrolidinium
RE	Reference electrode
RTIL	Room temperature ionic liquid
SEI	Solid electrolyte interphase
SIB	Sodium-ion battery
SL	Surface layer
SO_4^{2-}	Sulfate
SPE	Solid polymer electrolyte
TFSI	Bis(trifluoromethanesulfonyl)imide
T_g	Glass transition temperature
T_m	Melting temperature
TGA	Thermal gravimetric analysis
VTF	Vogel-Tamman-Fulcher
WE	Working electrode

List of Figures

Figure 1. Schematic of a SIB containing a hard carbon (HC) anode and a layered cathode. The anions in the electrolyte are omitted for sake of clarity.

Figure 2. Schematic of: a) lithiated graphite and b) sodiated hard carbon.

Figure 3. Schematic of: a) a layered oxide and b) a polyanionic based 3D structures. Inspired by [51] and [52], respectively.

Figure 4. Chemical structures of: a) DMC, b) DEC, c) EMC, d) EC and e) PC.

Figure 5. Scheme of the Mickey MouseTM anion concept.

Figure 6. Chemical structures of anions and cations from **II-V**: a) TFSI, b) FSI, and c) MM441 anions, and d) Pyr₁₃ cation.

Figure 7. Chemical structure of PEO.

Figure 8. Schematic energy diagram of: a) thermodynamic stability of the electrolyte and b) kinetic stability by formation of an SEI and an SL layer. Inspired by [135].

Figure 9. Schematic representation of the influence of the salt concentration on the σ for: a) SPE and b) LE. Inspired by [144] and [72], respectively.

Figure 10. Arrhenius plots for selected liquid and solid sodium based electrolytes: a) 1.5 m MM441 in H₂O **II**, b) 0.8 m NaTFSI in EC-PC (1:1) [58], c) NaTFSI 0.8 m in Pyr₁₃TFSI [58], d) NaTFSI(PEO)₉ - 20 wt% Pyr₁₃TFSI **V**, e) NaTFSI(PEO)₉, and d) NaTFSI(PEO)₂₀ **III**.

Figure 11. Arrhenius plot for NaFSI(PEO)₉ in the a) cooling and b) heating scan.

Figure 12. Simplified representation of the ionic conduction mechanisms in different electrolytes: a) vehicular in organic liquid based electrolytes, where the Na⁺ moves together with the first solvation shell, b) solvent exchange in organic liquid based electrolytes, where the Na⁺ conduction takes place with exchange of solvent molecules, c) vehicular in IL based electrolytes, d) exchange mechanism in IL based electrolytes, e) intrachain polymer segmental motion in SPEs, in which the Na⁺ motion is coupled to the PEO dynamics, and f) intrachain polymer segmental motion in ternary polymer electrolytes.

Figure 13. a) Liquid electrolyte and b) self-standing SPE film.

Figure 14. Schematic of a DSC furnace.

Figure 15. DSC heating traces for NaFSI(PEO)_n (*n*: 6, 9, 20). 1st scan (—), 2nd scan (---).

Figure 16. Schematic of a TGA apparatus.

Figure 17. Typical TGA plot with the graphical determination of T_{1%} and T_{onset} shown.

Figure 18. Schematic of the Raman effect. Rayleigh scattering is shown for comparison. Inspired by [183].

Figure 19. Raman spectra for NaFSI(PEO)_n (n: 6, 9, 20) in the range 700-770 cm⁻¹. The arrows indicate bands of “free” FSI, ion pairs and aggregates.

Figure 20. Fitting of the band assigned to the expansion-contraction mode of the TFSI anion in NaTFSI(PEO)₂₀. The Voigt profile and the Gaussian profile were used to fit the “free” TFSI anion and the CIPs, respectively.

Figure 21. Raman spectra for NaTFSI(PEO)_n (n: 6, 9, 20) in the range 800-880 cm⁻¹.

Figure 22. Schematic of IR photon absorption.

Figure 23. ATR working principle.

Figure 24. CV for the Me₁₀Fc⁺⁰ couple (~5 mM) in NaTFSI(PEO)₉ registered at 20 mVs⁻¹ on a Pt disc. A Na metal ring was used as RE.

Figure 25. Phase shift between a sinusoidal voltage and its response current.

Figure 26. Impedance plot, for a fixed frequency, in the complex plane. |Z| and ϑ are the module and the phase of the impedance, respectively.

Figure 27. Scheme of an EC used to simulate a cell with blocking electrodes (inspired by [193]).

Figure 28. Simulated impedance from the EC depicted in Figure 27 (inspired by [193]).

Figure 29. Impedance response for a SPE / blocking electrode cell.

Figure 30. Impedance response for a liquid electrolyte / blocking electrode cell.

Figure 31. Equivalent circuit used for analyzing the impedance data for a three-electrode cell comprising sodium metal as WE and NaTFSI(PEO)₉ as electrolyte **IV**.

Figure 32. Calculated capital costs for different LIBs and SIBs. Reproduced from **I** with permission from the Royal Society of Chemistry.

Figure 33. ESW for NaMM4411 and LiMM4411 based aqueous electrolytes. Reproduced from **II** with permission from the Royal Society of Chemistry.

Figure 34. Arrhenius plots for NaTFSI(PEO)_n and NaFSI(PEO)_n with n:6, 9, and 20. Reproduced from **III**.

Figure 35. Half-wave potential of the Me₁₀Fc^{+/-} redox couple in NaTFSI(PEO)₉.

Figure 36. Arrhenius plots of ionic conductivities for cooling (—) and heating (- - -) scans of: a) NaTFSI(PEO)₉ and NaTFSI(PEO)₉ – Pyr₁₃TFSI and b) NaFSI(PEO)₉ and NaFSI(PEO)₉ – Pyr₁₃FSI. Lines are a guide to the eye only. Reproduced from **V**.

List of Tables

Table 1. Comparison of various Na⁺ conducting electrolytes.

Table 2. Properties of liquid solvents commonly used in non-aqueous SIBs. T_m, T_b, η and ε are the melting temperature, the boiling temperature, the viscosity, and the dielectric constant, respectively. Data obtained from **I**.

Table 3. Viscosities of selected pyrrolidinium and imidazolium based ILs.

Table 4. Ionic conduction mechanisms of electrolytes.

Table of contents

Abstract	I
List of Publications	III
Contribution Report	IV
List of Acronyms	V
List of Figures	VI
List of Tables	VIII
1 Introduction	1
2 Batteries	3
2.1 Sodium Batteries.....	4
2.1.1 Anodes	5
2.1.2 Cathodes	6
3 From Liquid to Polymer Electrolytes	9
3.1 Organic Liquid Based Electrolytes	11
3.2 Aqueous Electrolytes	13
3.3 Ionic Liquid Based Electrolytes	15
3.4 Polymer Based Electrolytes.....	16
3.5 The Interface Electrode / Electrolyte.....	17
3.6 Ionic Conduction in Liquid and Polymer Electrolytes	19
4 Materials and Experimental Techniques	25
4.1 Preparation of Electrolytes	25
4.2 Thermal Analysis Methods.....	27
4.2.1 Differential Scanning Calorimetry	27
4.2.2 Thermal Gravimetric Analysis	28
4.3 Vibrational Spectroscopy.....	30
4.3.1 Raman Spectroscopy	30
4.3.2 Infrared Spectroscopy.....	33
4.4 Electrochemical Methods	34
4.4.1 Potentiodynamic Methods	34
4.4.2 Alternating Current Techniques	35
4.4.2.1 Ionic Conductivity of Electrolytes	37
4.4.2.2 Evaluation of the Interface Electrode / Electrolyte	40

4.4.3 Karl Fischer Coulometric Titration	40
5 Summary of appended papers	41
6 Conclusions and Outlook.....	47
Acknowledgements.....	48
Bibliography	49

1 Introduction

Batteries are part of our everyday life. In the domestic framework, we are surrounded by portable consumer electronics powered by batteries. In the automotive field, it is increasingly popular to power vehicles by batteries. The *electromobility* is undeniably an emerging field and comprises hybrid and fully electric vehicles [1]. Currently, lithium-ion batteries (LIBs) [2] have a high popularity owing to the high specific energy, $\sim 210 \text{ Wh kg}^{-1}$ [3]. Other applications of LIBs could include large-scale grid energy storage of renewable energy resources *e.g.* solar, wave, wind, *etc.* [4]. However, it is foreseen that, in near future, the actual production of lithium will not be able to satisfy the increasing market demand, which will lead to a higher price [5,6]. Thus, there is a driving force for developing new battery chemistries to replace/complement LIBs. The quest for new battery concept will affect the choice of all the battery components *e.g.* electrodes, electrolytes, and current collectors. By looking at the periodic table, the elements that show similar chemical and electrochemical properties to lithium are sodium and magnesium. The sodium resources are abundant, therefore sodium-ion batteries (SIBs) are potentially more sustainable in a long-term perspective **I**. Furthermore, copper current collectors (costly, heavy) used in commercially available LIBs can be replaced by aluminum (cheap, light) in SIBs, making sodium based chemistry even more appealing and there is no reason to assume that the final performance of SIBs will not be competitive to LIBs [7].

Common electrolytes used in LIBs and SIBs contain fluorinated salts, *e.g.* LiPF_6 and NaPF_6 , respectively, dissolved in liquid organic solvents. These electrolytes are usually accompanied by many intrinsic safety concerns [8], such as leakage of harmful liquids and gassing, thus requiring special battery packing and safety devices [9]. Although manufacturers and researchers aim to reduce cell failure and the safety level of commercial batteries is quite high on a single cell level [9], safety is still an issue in the automotive industry, where hundreds of cells are packed into modules and failure rate becomes critical [10,11].

Aiming to improve the battery safety, fluorine-free and non-flammable electrolytes should be developed. Alternative solvents could be water or a polymer - such as in a solid polymer electrolyte (SPE). The former has a large drawback in only enabling cells with low cell voltages, $\sim 2\text{V}$ [12] due to water decomposition, resulting in a low energy density. However, sodium aqueous batteries are being commercialized [13]. The latter alternative can be part of all-solid-state batteries often with a larger potential and specific energy than aqueous batteries. A variant of poly (ethylene oxide) (PEO) based SPEs is already used in the lithium metal polymer (LMP) battery at 100 Wh kg^{-1} powering the Bluecar; the electric car of the Autolib' car-sharing service in Paris, France [14]. Despite the increased safety, SPEs have some problems to overcome in order to make them the overall first-hand electrolyte alternative. The major issue is that SPEs show severely lower room temperatures (RT) conductivities than liquid electrolytes. For example, in order to guarantee suitable conductivity, the battery powering the Bluecar is operating at *ca.* $80 \text{ }^\circ\text{C}$. Therefore, current research aims to increase the close to RT ionic conductivity in different ways. One way is to

add an ionic liquid (IL) [15] to the SPE to create a ternary polymer electrolyte [16]. ILs have very low vapor pressures and have low flammability hazards, therefore not compromising the safety advantages [16–19].

This thesis focuses on different electrolyte components for sodium batteries. Fluorine-free salts have been proposed and evaluated in terms of basic physicochemical properties, in order to meet the increasing demand of safer liquid based electrolytes. Aiming at sodium all-solid-state batteries, SPEs comprising different sodium salts have been studied in terms of thermal properties, ionic speciation, ionic conductivity and compatibility *vs.* sodium metal. The effect of addition of ILs on the morphology, ionic speciation and ionic mobility of SPEs has also been investigated. The resulting overall picture allows a critical evaluation of advantages and drawbacks of electrolytes for sodium batteries.

2 Batteries

The first battery was invented by Alessandro Volta about two hundreds years ago [20]. It was composed of a pile of interleaved zinc and silver discs separated with brine-soaked leather or cardboard [21]. Since then, many different battery concepts and chemistries have been proposed. Batteries can be divided in two categories: primary and secondary. Primary batteries can supply energy only once through a discharge process - and are then discarded. Secondary, or more often rechargeable batteries, can supply electric energy for hundreds to thousands charge/discharge cycles. In Figure 1, a rechargeable SIB is schematically depicted. Henceforth only rechargeable batteries will be considered.

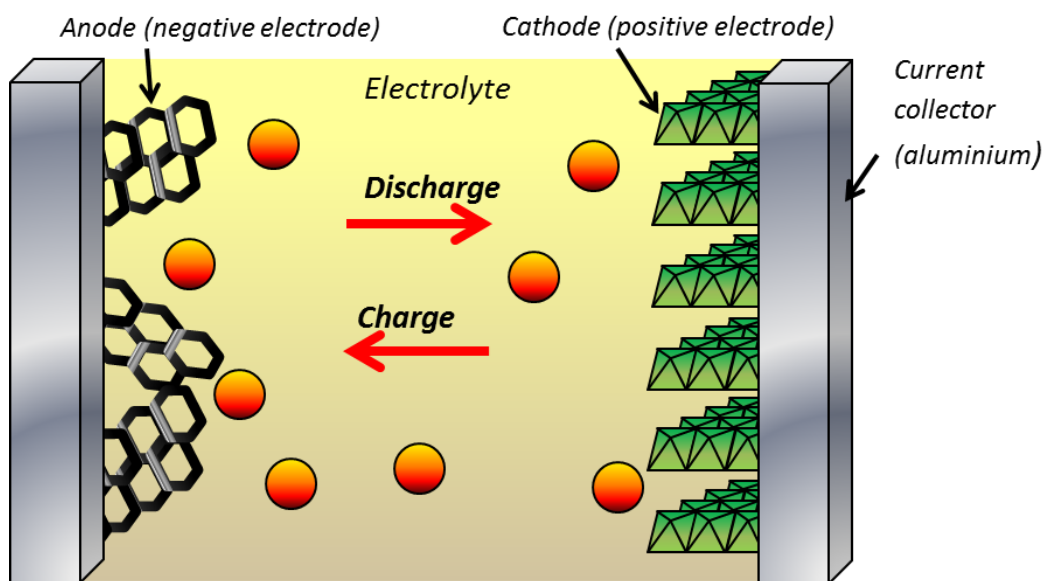


Figure 1. Schematic of a SIB containing a hard carbon (HC) anode and a layered cathode. The anions in the electrolyte are omitted for sake of clarity.

The lead-acid battery, invented by Gaston Planté [20] in 1859, shows some environmental and health concerns, mainly due to the use of lead [22,23] and has a low specific energy $\sim 35 \text{ Wh kg}^{-1}$ [24]. However, is still in use as starting-lighting-ignition (SLI) battery for vehicles due to its power rate and low price. The nickel-metal hydride (NiMH) battery is used both in portable electronics [25,26] and hybrid electric vehicles [27]. The NiMH battery shows only about half ($\sim 60 \text{ W kg}^{-1}$) the specific energy provided by a state-of-the-art LIB [24]. Commercial LIBs typically use graphite as anode and a metal oxide, originally LiCoO_2 , as cathode [2]. A solution of 1 M lithium hexafluorophosphate (LiPF_6) in carbonate based solvents such as ethylene carbonate (EC) and dimethyl carbonate (DMC) is the standard electrolyte which is absorbed by the separator - often a polyolefin membrane. This is called the “rocking chair battery” since the Li^+ transported through the electrolyte rocks between the two electrodes. A fully lithiated graphite anode, LiC_6 has a theoretical capacity of 372 mAh g^{-1} and is preferred over lithium metal anode (3860 mAh g^{-1}) as it does not have the

same issues related to severe dendrite formation, *e.g.* short circuit, which implies safety risks, *e.g.* fire. Today, graphite is still the first choice as anode material for LIBs, despite other anode materials have been proposed [28]. Metallic lithium can, though, be used as anode in solid-state batteries *e.g.* the Bluecar battery [14]. As for the cathode, LiCoO₂ is still the most common cathode but not as dominant as in the past, for portable electronics. Indeed, LiCoO₂ shows high cost, low thermal stability, and fast capacity fade during deep cycling [28]. Other materials used as cathodes in LIBs are for example, lithium nickel manganese cobalt oxide (LiNi_{1/3}Mn_{1/3}Co_{1/3}O₂) and lithium iron phosphate (LiFePO₄) [29].

More specifically, a *battery* is a device consisting of one or more electrochemical *cells* but in this thesis these two terms will be used interchangeably. In an electrochemical cell, chemical energy is transformed into electricity by reduction and oxidation (redox) reactions at two electrical conductors (electrodes). During discharge of an SIB as shown in Figure 1, oxidation takes place at the anode or negative electrode, here hard carbon (HC), while reduction takes place at the cathode or positive electrode. The process is inverted during charging. The current flow is determined by the potential difference between the cathode and the anode - the cell voltage. The two electrodes are separated by the electrolyte, an ionic conductor and electronic isolator (to avoid short-circuit), which is made by dissolving a salt into a matrix, the focus of this thesis.

2.1 Sodium Batteries

Sodium batteries include some very different technologies: SIBs (based on non-aqueous and aqueous electrolytes), Na-NiCl₂ (ZEBRA), Na-S, and Na-O₂. Among the commercially available batteries for the market of large-scale energy storage SIBs based on aqueous electrolytes are operating at room temperature [13], while both ZEBRA and Na-S batteries operate at high temperature $T > 270^{\circ}\text{C}$ [30]. The latter two, since they use liquid sodium as the anode, have to meet very stringent safety requirements [31,32].

In this thesis the focus is entirely on sodium batteries operated “close to room temperature (RT)”. These batteries can be divided in two main groups, on the basis of the anode: sodium metal batteries and SIBs. In the former the anode is sodium metal, and sodium ions will be deposited or stripped on/from it, while for the latter the working principle is the same as in LIBs. The research on these battery concepts started already in the 1980-90’s [33,34], more or less ceased when the LIBs became popular and commercialized, and has recently gained new momentum [35].

The knowledge gained from more than 30 years of R&D in the LIB field can be beneficial for SIBs, even if the choice of material can be limited by the type of ions (Li⁺ or Na⁺) that rock between the electrodes, see next paragraphs. There is today no commercial non-aqueous SIB, even though some prototypes have been made [36]. Electrolytes for sodium batteries operating “close to RT” will be the focus of the next chapter, but before a brief overview of relevant electrodes is given.

2.1.1 Anodes

First we distinguish between sodium metal anodes from all other sodium battery anodes. Also, to put the sodium batteries in perspective, we make comparisons with the anodes used in lithium batteries. Sodium metal has a theoretical capacity of 1166 mAh g^{-1} , about 30% of the theoretical capacity of lithium metal (3860 mAh g^{-1}). It has a melting point of $98 \text{ }^\circ\text{C}$ (Li melts at $180 \text{ }^\circ\text{C}$) and is more reactive to H_2O than lithium metal. This sets both a stringent upper limit in its operating temperature and raises safety concerns related to its usage. Nevertheless, sodium metal anodes are useful as they could provide high specific energy batteries. Among other anodes, we distinguish mainly between carbon based and inorganic compounds.

HC is the most popular carbon based material for SIBs. It can be obtained from many organic precursors [37,38] and, upon sodiation, it undergoes a small volume expansion. HC shows an insertion potential of $0.005 \text{ vs. Na}^+/\text{Na}$, thus close to the sodium deposition potential and hence a safety concern. Its structure is disordered (Figure 2) which enables the insertion of sodium ions but shows a lower theoretical capacity (300 mAhg^{-1}) than graphite for LIBs (372 mAhg^{-1}). However, Na^+ cannot intercalate in graphite - only recently expanded graphite was proposed as a suitable SIB anode [39].

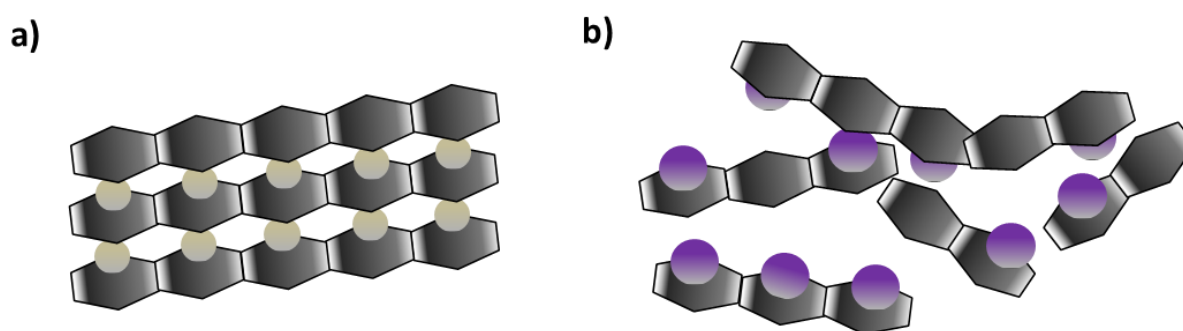


Figure 2. Schematic of: a) lithiated graphite and b) sodiated hard carbon.

The inorganic compounds used as anodes in non-aqueous SIBs are usually classified on the basis of the mechanism with which Na^+ reacts with the electrode; intercalation, alloying, or conversion reactions. This classification is the same as for LIB anodes. For intercalation anodes, the ions are inserted without changing its structure, and thus have a negligible small volume expansion upon sodiation. A typical example is $\text{Na}_2\text{Ti}_3\text{O}_7$ [40] with an insertion potential of *ca.* $0.3 \text{ V vs. Na}^+/\text{Na}$ and a capacity of 200 mAhg^{-1} . Alloying and conversion anode materials involve distinct structural changes upon reaction with Na^+ and the corresponding volume expansion is a strong limitation to their utilization [41]. However, in both cases the volumetric expansion for sodium based electrodes is higher than for the lithium analogues and this is due to the larger ionic radius of Na^+ compared to Li^+ . For a conversion anode as CuO , the volume expansion is $\sim 170 \%$ with Na^+ , while is $\sim 70 \%$ with Li^+ [42]. For alloying reaction, volumetric expansion, of 420% is reached for $\text{Na}_{15}\text{Sn}_4$, while for $\text{Li}_{22}\text{Sn}_5$ is 260% [43]. Other examples of conversion compounds are CoO and Co_3O_4 while for alloying

Pb and Sb have also been used [41,44]. For aqueous SIBs, NASICON type compounds (see next paragraph) such as $\text{NaTi}_2(\text{PO}_4)_3$ have been extensively investigated as anodes and have a theoretical capacity of 133 mAhg^{-1} and a voltage set at $2.1 \text{ V vs. Na}^+/\text{Na}$ for the redox couple $\text{Ti}^{4+}/\text{Ti}^{3+}$ [45].

2.1.2 Cathodes

Since no Na^+ is provided by any of the above SIB anodes, the SIB cathodes need to provide these. Here we distinguish between layered oxides and polyanionic based 3D structures (Figure 3). Layered oxides have the general formula Na_xMO_2 , where M is a transition metal. They can contain a single transition metal, as in NaCrO_2 , which exhibit reversible capacity of *ca.* 120 mAhg^{-1} , but shows reversible cycling only for x that ranges 0.5-1 in $\text{Na}_x\text{Cr}_{1-x}\text{O}_2$ [46]. Moreover, one polymorph of NaVO_2 showed also a reversible capacity close to 120 mAhg^{-1} but a too low potential of insertion, $2.4 \text{ V vs. Na}^+/\text{Na}$ [47]. NaMnO_2 exhibited a specific capacity of *ca.* 190 mAhg^{-1} but it also displayed large distortions which could led to poor cycling performance [48]. However, NaMnO_2 in its orthorhombic phase $\text{Na}_4\text{Mn}_9\text{O}_{18}$ was proven to be a suitable cathode in aqueous SIBs, with excellent electrochemical stability (over 1000 cycles), despite it was only able to deliver 45 mAh g^{-1} [49]. Since single-transition metal oxides did not exhibit suitable practical application for non-aqueous SIBs, the research has focused on compounds containing multiple transition metal atoms. Among those, $\text{Na}[\text{Mn}_{1/4}\text{Fe}_{1/4}\text{Co}_{1/4}\text{Ni}_{1/4}]\text{O}_2$ has an initial discharged capacity of 180 mAhg^{-1} at an average voltage of 3.2 V [50].

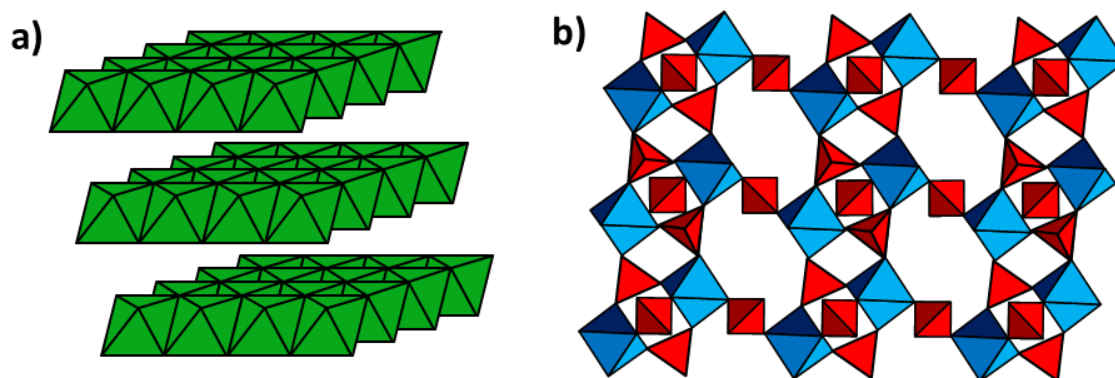


Figure 3. Schematic of: a) a layered oxide and b) a polyanionic based 3D structures. Inspired by [51] and [52], respectively.

Polyanionic compounds consist of 3D frameworks, built from a combination of tetrahedral XO_4 ($\text{X}=\text{P},\text{S}$) and octahedral MO_6 showing long-term structural stability [52]. NaFePO_4 , while in its maricite form is electrochemically inactive, in its olivine-type structure is electrochemically active exhibiting a theoretical capacity of 154 mAh/g and an average potential, due to the $\text{Fe}^{3+}/\text{Fe}^{2+}$ redox couple of 3 V vs. Na^+/Na [52]. Another example of polyanionic compounds is NASICON (Na Super Ionic CONductor), [41,52] originally developed as a solid electrolyte, with the general formula $\text{Na}_x\text{M}_2(\text{PO}_4)_3$ which exhibit poor electronic conductivity. Among them, $\text{Na}_3\text{V}_2(\text{PO}_4)_4$ (NVP) was proposed already in the 80's [53] and its electrochemical activity mostly relies on the redox couple $\text{V}^{4+}/\text{V}^{3+}$ located at 3.4 V vs. Na^+/Na . In order to increase its conductivity, NVP can be carbon coated, as done in [54], where the composite cathode showed a practical capacity of about 93 mAhg⁻¹ with organic liquid based electrolytes. Moreover, NVP was used to build a HC NVP full cell [7]. Another 3D compound is the fluorophosphate $\text{Na}_3\text{V}_2(\text{PO}_4)_2\text{F}_3$, or NVPF, which showed a specific capacity as high as ~120 mAhg⁻¹ [55]. Research on electrodes for sodium batteries has proposed several materials that show similar working mechanisms as for lithium batteries. However, sodium and lithium based electrodes show differences, mainly due to the larger size of Na^+ to Li^+ , in their chemical composition and structures. Overall, the performance of the state-of-the-art SIB anodes and cathodes are still behind the lithium analogues, but it is foreseen that they will improve [41].

3 From Liquid to Polymer Electrolytes

As mentioned in Chapter 2, the electrolyte provides the ionic transport between the cathode and the anode and it usually consists of a source of Na^+ and a medium, a solvent, in which the Na^+ moves. The electrolyte should have a high ionic conductivity (σ), at least $10^{-3} \text{ S cm}^{-1}$ at room temperature (RT) in order to obtain good performance in consumer battery systems [56]. The electrolyte must also be an electronic insulator, to avoid short-circuit of the cell (electronic conductivity $< 10^{-10} \text{ S cm}^{-1}$). Moreover, the electrolyte should also:

- Show a large chemical stability and wide electrochemical stability window (ESW).
- Be able to minimize concentration polarization phenomena.
- Be non-toxic and environmentally “friendly”.

<i>Electrolyte</i>	<i>Example</i>	<i>ESW (V)</i>	<i>Thermal stability</i>	<i>Conductivity at RT (S cm^{-1})</i>	<i>Reference</i>
Organic	0.5 M NaPF_6 in $\text{EC}_{0.3}:\text{DMC}_{0.7}$	~4.5	+	$\sim 6 \cdot 10^{-3}$	[57]
Aqueous	1.5 m NaMM4411 in H_2O	~2	++++	$\sim 3 \cdot 10^{-2}$	II
IL	0.8 m NaTFSI in $\text{Pyr}_{13}\text{TFSI}$	~4	+++	$\sim 2 \cdot 10^{-3}$	[58]
SPE	$\text{NaFSI}(\text{PEO})_{20}$	~4.5	+++	$\sim 10^{-7}$	[59]
Ceramic	Na_3PS_4	~5	++++	$\sim 10^{-4}$	[60]

Table 1. Comparison of various Na^+ conducting electrolytes.

The ESW is determined by the extent of oxidation and reduction reactions. The ESW is a key factor in determining which kind of electrolyte is suitable for a certain combination of electrodes. The assessment of the ESW strongly depends on the electrodes employed, the measurement conditions and the evaluation criteria. As a rule of thumb, the wider the ESW, the higher is the energy density that the battery can offer - as then electrode materials with an increased voltage difference can be chosen.

The electrolyte should in general not decompose in the battery, but for instance the success of non-aqueous LIBs relies on a protective layer on the electrode surface formed by controlled partial decomposition of the electrolyte. The protective layer formed on the negative electrode is denoted as the solid electrolyte interphase (SEI) [61–63], while that on the positive electrode is called the surface layer (SL) [64,65] and will both be described in section 3.5.

The use of liquid electrolytes in an electrochemical cell is always connected with the use of a separator, to physically separate the electrodes and to provide a suitable mechanical stability to the cell. The separator can be made of different materials and its choice depends on several factors as wettability, porosity, thickness, pore-size, mechanical strength, chemical and thermal resistance [66]. Polyolefin based membranes [67] are often used together with non-aqueous electrolytes with low viscosity (η), while glass fiber based separators can be used with high η electrolytes, *e.g.* based on ionic liquids (ILs, see next section). In aqueous SIBs, non-woven cotton or synthetic fiber filtration papers are employed [12]. However, no separator is necessary with the use of a polymer electrolyte or a ceramic electrolyte as they themselves act as separators. Polymer electrolytes often guarantee a better contact electrode/electrolyte than ceramics.

Overall, the chemical and physical natures of the solvents and the salt(s) play an important role in assessing the solubility of the latter. The thermodynamics of the dissolution process is determined by an interplay of different solvent and salt properties. Among the factors that affect the dissolution process there are the following:

- Disorder of the ions as they move from the ordered crystalline structure of the Na-salt to the solution.
- The rearrangement of the solvent molecules during dissolution of the salt.
- Lattice enthalpy of the salt.
- Electrostatic interactions between dissolved ions.
- Solvation of the cations by interaction with the solvent molecules.
- Enthalpy of dissolution due to the ability of the solvent to weaken the interactions between the anion and cation.

The following sections will deal with liquid and polymer electrolytes.

3.1 Organic Liquid Based Electrolytes

While aqueous SIBs and LIBs share similar electrolytes since they are both water based [68], organic liquid based SIBs and LIBs contain different solvents. Indeed, some solvents used for electrolytes of LIBs may not be suitable for SIBs since they do not form well-behaving SEI or SL layers. Moreover, Na^+ is a weaker Lewis acid than Li^+ and so its interaction with the anions of the salt is expected to be weaker - which might impact on the solvents selection, the ideal salt concentration, and also the SEI formation. For both LIBs and SIBs, the most intensively studied liquid electrolytes are based on linear and cyclic carbonates (Figure 4). Propylene carbonate (PC) is the most used solvent for SIBs which is in contrast to LIBs, where PC co-intercalates into graphite and leads to its exfoliation. However, PC has to be used in combination with other solvents, *e.g.* ethylene carbonate (EC) to produce a stable SEI on HC [69,70]. There is a wide range of binary solvent based electrolytes: EC/dimethyl carbonate (DMC) [70], EC/diethyl carbonate (DEC) [70] and DMC/EC/PC [7]. The dielectric constants of organic liquid solvents vary between 90 (EC) and 2.8 (DMC) (Table 2) and in general solvents with higher dielectric constants can better dissolve the Na-salts. DMC or DEC are used to decrease the viscosity and increase the ionic conductivity of the electrolyte (see section 3.6), as their $\eta_{25\text{ }^\circ\text{C}}$ is $<1\text{ mPa s}$ (Table 2). All the solvents mentioned above are liquids at RT, except EC that melts at $\sim 35\text{ }^\circ\text{C}$. The flammability issues connected with the use of organic liquids can be mitigated via addition of ILs (section 3.3), to obtain hybrid electrolytes [58].

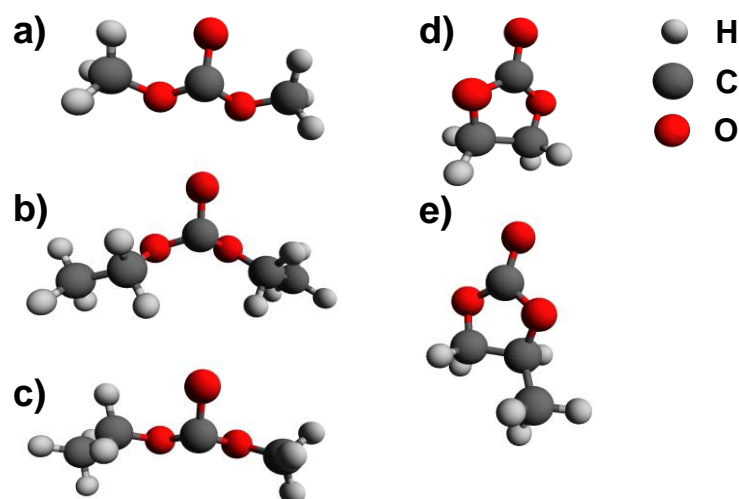


Figure 4. Chemical structures of: a) DMC, b) DEC, c) EMC, d) EC and e) PC.

<i>Solvent</i>	<i>Melting Temperature</i> T_m (°C)	<i>Boiling Temperature</i> T_b (°C)	<i>Viscosity at 25 °C</i> η (mPa s)	<i>Dielectric constant</i> ϵ
Dimethyl carbonate (DMC)	4.6	91	0.59	3.1
Diethyl carbonate (DEC)	-74	126	0.75	2.8
Ethyl methyl carbonate (EMC)	-53	110	0.65	3.0
Ethylene carbonate (EC)	36	248	1.9 (40 °C)	90
Propylene carbonate (PC)	-49	242	2.5	66

Table 2. Properties of liquid solvents commonly used in non-aqueous SIBs. T_m , T_b , η and ϵ are the melting temperature, the boiling temperature, the viscosity, and the dielectric constant, respectively. Data obtained from **I**.

The most used salt in the formulation of liquid non-aqueous electrolytes for SIBs is sodium hexafluorophosphate, (NaPF₆), chosen for its performance in terms of ionic conductivity and SEI formation, and also because it decomposes to F⁻ which passivates the aluminium current collectors. Also other salts that have been proposed are usually the sodium versions of the salts investigated in the field of lithium batteries: sodium tetrafluoroborate (NaBF₄), sodium perchlorate (NaClO₄), sodium trifluoromethanesulfonate (NaCF₃SO₃), sodium bis(trifluoromethanesulfonyl)imide (NaTFSI) and sodium bis(fluorosulfonyl)imide (NaFSI). For solvents, another class consists of glymes, with the general formula CH₃O(CH₂CH₂O)_n-CH₃. Liquid electrolytes comprising of NaPF₆ and mono (n=1), di (n=2), and tetra (n=4) glymes have enabled non-dendritic sodium plating and stripping [71].

Ponrouch *et al.* [69] evaluated basic physicochemical and electrochemical properties of 1 M solutions of NaClO₄, NaTFSI and NaPF₆ in different solvents such as EC, PC, DMC, DME, DEC and triglyme and their mixtures: EC:DMC, EC:DME, EC:PC and EC:Triglyme. A 1 M solution of NaPF₆ in EC_{0.5}:PC_{0.5} was found to be an optimum, even in respect to an HC anode. Bhide *et al.* [57] investigated the electrochemical performance of NaCF₃SO₃, NaPF₆ and NaClO₄ at different concentration in a EC_{0.3}:DMC_{0.7}. Also in this case the NaPF₆ based electrolyte outperformed the other and tested with a Na_{0.7}CoO₂ positive material led to the formation of a stable surface layer. Very recently, salts based on heterocyclic rings such as NaTDI and NaPDI have also been proposed [72], which seem promising since they showed high thermal stabilities, excellent resistance versus moisture, and their 1 M solution in PC exhibited conductivities of $\sim 4 \cdot 10^{-3}$ S cm⁻¹ at 20 °C [72].

TFSI (Figure 6a) is a popular anion, and the most studied anion for solid polymer electrolytes (SPEs) (see section 3.4) ever since the introduction of LiTFSI in the 1980's [73,74]. This flexible anion has a combination of size and large degree of charge delocalization that results in plasticizing properties, mitigating the usual increase in glass transition temperature (T_g) observed upon addition of a salt to a polymer to create an SPE [74–77]. Furthermore, the low lattice energy of TFSI based salts favor dissociation, particularly important in a polymer matrix. Once solvated, the formation of ion pairs and high ordered aggregates (see section 3.6) is lower **III**, due to much weaker ion-ion interactions as compared to *e.g.* triflate [78–80] or FSI based SPEs **III**. Moreover, NaTFSI was recently used in liquid electrolytes [81,82]. LiTFSI was also used for the preparation of water-in-salt electrolytes [83], see chapter 4. The FSI anion (Figure 6b) has many similar basic characteristics to the TFSI anion - including similar weak ion-ion interactions [84]. NaFSI, Na[N(FSO₂)₂], has been tested only recently in liquid electrolytes [85–87], in SPEs **III**, [59], and in ternary polymer electrolytes, **V**.

All the anions of the above mentioned salts have drawbacks. For example, ClO₄⁻ is a strong oxidant, BF₄⁻ has strong interaction with the cation, therefore results in less conductive electrolytes; CF₃SO₃⁻ interacts strongly with the cation and also corrodes the aluminum current collectors. PF₆⁻ has safety issues at high temperature and in presence of moisture, suffering from hydrolysis that gives corrosive and toxic species, *e.g.* HF. TFSI shows corrosion problems of the aluminum current collectors when used in liquid based electrolytes [81], but in SPEs studies on lithium polymer batteries show this is only significant during overcharging [88]. The FSI anion does not show clear behavior with respect to aluminium corrosion as it is not well established if the observed corrosion has been due to impurities in the salt (as Cl⁻) or to the FSI anion itself [89,90]. In general, sodium salts show higher melting points and larger thermal stabilities than the lithium analogues. Overall, considering possible decomposition reactions, corrosion issues, *etc.* the choice of suitable, high purity and dry salts are delicate matters [91].

3.2 Aqueous Electrolytes

Water is cheaper and easier to obtain than organic solvents and was employed in the first batteries [20] and is the most common protic solvent. It has a high relative dielectric constant (ϵ *ca.* 80), which favors dissolutions of many salts. Additionally it has also a low viscosity at 25 °C ($\eta_{25\text{ °C}}$) of 0.89 mPa s [92], contributing to the highest room temperature (RT) conductivities among liquid electrolytes. Its main drawback is its narrow ESW which, due to thermodynamics considerations, is set at ~1.23 V [93]). However, aqueous SIBs can operate in a voltage range of *ca.* 2 V [12] due to kinetic reasons, such as sluggish electron transfer or formation of a SEI or SL. Nevertheless, it is well established that for practical battery applications, the ESW of aqueous electrolytes is narrower than for aqueous electrolytes, **I**, **II**, [12]. Anions that have often been used in aqueous electrolytes for SIBs are mostly inorganic: sulfonate (SO₄²⁻), nitrate (NO₃⁻), [12,68,94] and perchlorate ClO₄⁻ [95]. The first anion among the three is preferred over the other two since it does not show the same safety issues – *i.e.* it is not a strong oxidant and shows better thermal stability.

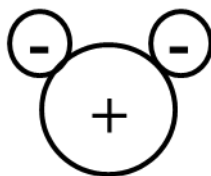


Figure 5. Scheme of the Mickey Mouse[™] anion concept.

In paper **II**, a new class of organic anions was proposed for use in aqueous SIBs. The concept of pseudo-localized anions, termed also as Mickey Mouse[™] (MM) anions (Figure 5), was introduced in [96] via molecular modelling studies that focused on Li⁺ based fluorine-free salts. In these anions, the charge is neither delocalized nor localized to a particular region of the molecule (Figure 5). Sodium (di-methyl ammonio)bis(butane-1-sulfonate) (NaMM4411, Figure 6c), was the first synthesized sodium based pseudo-localized salt, due to its easier synthesis compared to the other proposed anions. The NaMM4411 has proven to be soluble in water (up to 5 m) and its aqueous based electrolytes showed similar ESWs to electrolytes based on SO₄²⁻ and NO₃⁻ using similar electrodes [97]. However, NaMM4411 showed very poor solubility in common non-aqueous solvents and even in PEO, likely due to the salt's high dissociation energy (~800 kJmol⁻¹), the highest among the proposed anions [96].

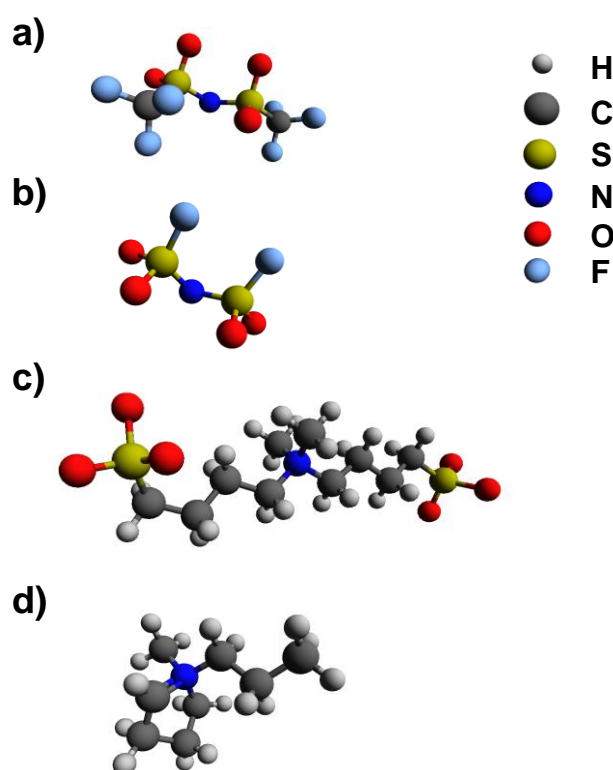


Figure 6. Chemical structures of anions and cations from **II-V**: a) TFSI, b) FSI, and c) MM4411 anions, and d) Pyr₁₃ cation.

3.3 Ionic Liquid Based Electrolytes

Ionic liquids (ILs) have recently been proposed as solvents for sodium battery electrolytes [98,99]. An IL is not only a solvent, it is also a salt that is liquid at $<100\text{ }^{\circ}\text{C}$ [100], and thus contains a large number of charge carriers. When the T_m is below RT, the name “room temperature ionic liquids” (RTILs) is preferred but in this thesis they will simply be referred to as ILs. ILs based on the pyrrolidinium (Pyr) and imidazolium (Im) cations are often used for SIB electrolytes. Since common ILs do not contain Na^+ , addition of a sodium source (Na-salt) is necessary to create a sodium battery electrolyte. This addition decreases the ionic conductivity of the IL [98], but conductivities above 10^{-3} Scm^{-1} at RT can still be obtained. Indeed, Na^+ interacts strongly with the IL anions [98], contributing to increased viscosities and a decreased ionic mobility of the electrolytes. The viscosities of ILs are usually much higher than those of organic liquids (Tables 2 and 3). On the other hand, they show much lower vapor pressures, hence enhanced safety [15]. Upon addition of an IL to a SPE, a ternary polymer electrolyte is obtained, which was proven to be a successful approach for Li systems [16,101], to improve the polymer dynamics (see section 3.6) as compared to the base SPE, and is here proposed for the sodium analogues in **V**.

<i>IL</i>	<i>Viscosity at 20 °C η (mPa s)</i>	<i>Density at 20 °C (g mL⁻¹)</i>	<i>σ at 20 °C (S cm⁻¹)</i>	<i>Reference</i>
Pyr ₁₃ TFSI	89	1.48	$1.47 \cdot 10^{-3}$	[58,102]
Pyr ₁₃ FSI	66	1.33	$8 \cdot 10^{-3}$	[102,103]
EmImTFSI	40	1.52	$8.9 \cdot 10^{-3}$	[98]
BMImTFSI	64	1.44	$3.5 \cdot 10^{-3}$	[98]

Table 3. Properties of selected pyrrolidinium and imidazolium based ILs.

Some typical pyrrolidinium based ILs for sodium battery electrolytes are: N-methyl-N-butylpyrrolidinium TFSI (Pyr₁₄TFSI) [104], N-methyl-N-propylpyrrolidinium FSI (Pyr₁₃FSI) [99], N-methyl-N-propylpyrrolidinium TFSI (Pyr₁₃TFSI) [58]. Among the imidazolium based ILs there are: 1-ethyl-3-methyl Imidazolium TFSI (EmImTFSI) [98,105] and 1-butyl-3-methyl imidazolium TFSI (BmImTFSI) [98]. Pyrrolidinium based electrolytes usually show lower conductivities [98,104], but better electrochemical stabilities than imidazolium based electrolytes [106].

3.4 Polymer Based Electrolytes

Polymers are considered as suitable solvents for battery electrolytes due to their mechanical properties as well as thermal and chemical stability. They were originally proposed for lithium metal batteries, because of their ability to stabilize the anode surface. Polyethers were the first polymers seriously considered since they excellently dissolve Na^+ despite having a low ϵ of ~ 5 -10 [32]. This is due to the Na^+ interactions with ether oxygen atoms ($\text{Na}^+\text{-O}$), which can be explained in terms of the “hard and soft acids bases” (HSAB) theory [107]. PEO, which consists of ethylene oxide repeating units (Figure 7) has been the most studied polymer to make SPEs since the discovery of its ability to complex alkali metal ions by Fenton *et al.* [108]. SPEs based on PEO were proposed for lithium batteries already in 1979 [109] and were used for sodium batteries in the 1980’s [110,111]. Early studies performed during the 80’s dealt mainly with studies in full cells with PEO- NaClO_4 system [111,112], while in the 90’s they focused also on the PEO- NaCF_3SO_3 [113,114] and PEO- NaTFSI [76,115]. The latter has also been investigated in **III** and **IV**. The especially strong solvating properties of PEO are due to the oxygen atom interspacing that allows for easy wrapping of the PEO chains around the cations without excessive stress. This is not the case for poly (methylene oxide) (PMO) or poly (propylene oxide) (PPO).

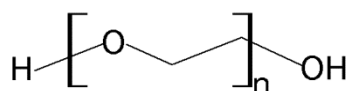


Figure 7. Chemical structure of PEO.

The molecular weight (MW) employed for SPE is typically 10^6 . The influence of the end-groups, OH on the conductivity can be disregarded for MWs above the entanglement limit [116], which for PEO is ca. $3200 - 5870 \text{ g mol}^{-1}$ [117]. The PEO used in **III** - **V** has a MW of $5 \cdot 10^6$ and semi-crystalline morphology, with a melting temperature (T_m) of ca. $68 \text{ }^\circ\text{C}$ and T_g of ca. $-50 \text{ }^\circ\text{C}$. These properties are useful as starting points, but can be drastically modified upon the creation of SPEs, **III**, and ternary polymer electrolytes, **V**. However, the PEO based SPEs are usually semi-crystalline with the crystalline phase due to PEO or to crystalline complexes between the PEO and the salt [118].

The amount of salt and the species of the anion in the polymer electrolyte drastically affects the morphology of the SPE. For this reason, it is fundamental to evaluate the most suitable composition for each combination of salt and polymer - most often PEO. A common way to identify the SPE composition is to consider the molar ratio between the PEO ether oxygen atoms and Na^+ , (O/Na), often denoted by n , instead of the salt wt% or the molar concentration. There is no standard n value since the morphology and ionic speciation in an SPE strongly depends on the used salt. SPEs with different composition, n : 6, 9, 20, which correspond to molalities, m , (see Chapter 4) of: 3.8, 2.5 and 1.1, respectively, were evaluated in **III**.

The T_g of an SPE can be lowered with addition of a plasticizer which has been termed as a substance that is incorporated into a material to increase its flexibility and workability [119]. The term plasticizer [120] is usually adopted for describing compounds effective in modifying the mechanical properties of amorphous plastic materials as *e.g.* PVC. Turning to SPEs, the definition of a plasticizer is mainly related to conductivity; a plasticizer can be described as a chemical species that improves the close to RT conductivity of a polymer electrolyte by increasing the amorphous phase and the chain dynamics. Plasticizers for SPEs can be low molecular weight organic molecules such as liquid carbonates [121], plastic crystals [122,123] and ions [74], **I**, **III**. In the latter case, the plasticizing species can be introduced directly with the sodium salt - such as TFSI or NaTFSI, where this suitable choice of anion can mitigate/soothe the cross-linking effect of the Na^+ **I**, **III**. Another option is to introduce plasticizing anions and cations via addition of ionic liquids (ILs) **V**.

Another polymer based electrolyte concept is gel polymer electrolytes (GPEs). GPEs were firstly introduced for LIBs [124], but are much less studied for SIB applications. They usually comprise a polymer and a liquid electrolyte, up to ~250 wt% [125] and for this reason, they usually show higher conductivities, *e.g.* $\sim 6 \cdot 10^{-3} \text{ S cm}^{-1}$ [126]. Polymers that have been proposed so far for SIBs are: poly(vinylidene fluoride - hexafluoro propylene), PVdF/HFP, [125,127] and poly(methyl meta)acrylate, PMMA [126].

3.5 The Interface Electrode / Electrolyte

The electrolyte components, in contact with two electrodes, are thermodynamically stable if their lowest unoccupied molecular orbital (LUMO) and highest occupied molecular orbital (HOMO) are higher and lower than the energy of the anode and the cathode, respectively (Figure 8a). When the energy of the anode and the cathode is higher and lower than the energy of the LUMO and HOMO of the solvent and the salt, respectively, the electrolyte will decompose since it is not thermodynamically stable (Figure 8b). The decomposition of the electrolyte can produce a protective layer on the electrode surface: the solid electrolyte interphase (SEI) [61–63] on the anode and the surface layer (SL) [64,65] on the cathode, respectively. These layers, with thicknesses $< 100 \text{ nm}$ [128,129] are permeable to the Na^+ and are mainly formed by reduction and oxidation of the electrolyte, respectively. However, the conductivities in these layers is quite low, estimated as $\sim 10^{-8} - 10^{-10} \text{ Scm}^{-1}$ for the SEI [130]. In order to obtain a kinetic stable SEI or SL, the choice of suitable electrolyte components is pivotal and the protective layer can be further improved through the addition of fluorinated additives [131].

The evaluation of the SEI composition is often complex since the analytical procedure and measurements conditions can dramatically affect the outcome. Indeed, techniques such as x-ray photon electron spectroscopy (XPS) and FTIR spectroscopy (see chapter 4), often used for the SEI chemical characterization, usually require the removal of the anode from the cell, and its transfer to the instrument [63,65].

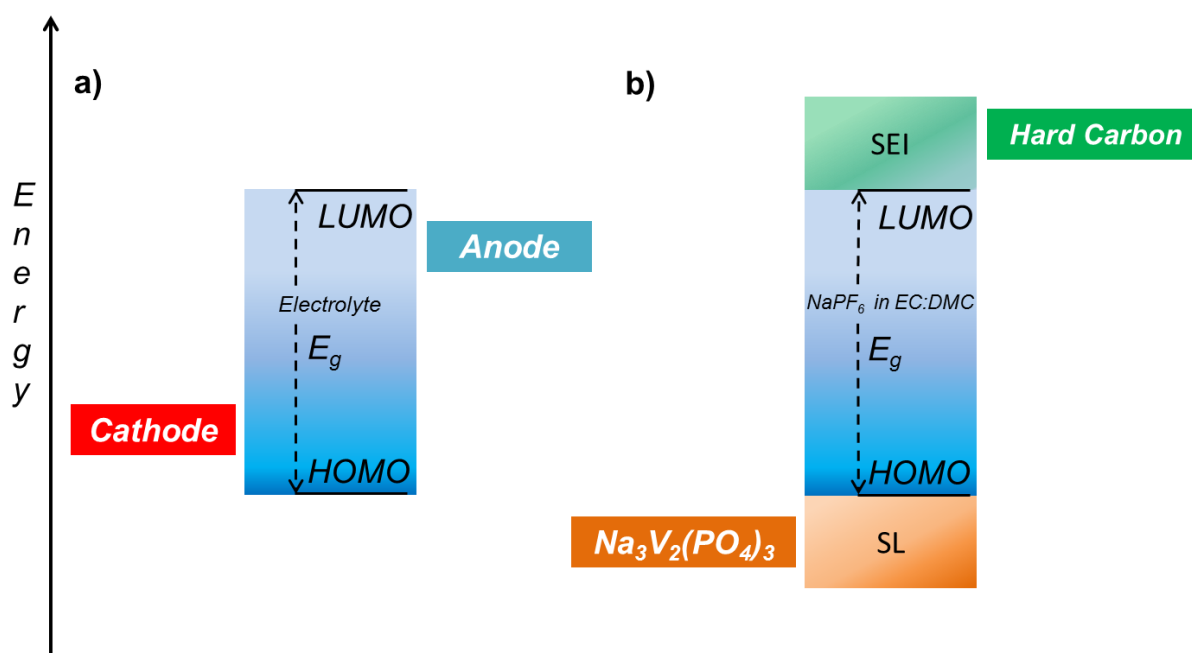


Figure 8. Schematic energy diagram of: a) thermodynamic stability of the electrolyte and b) kinetic stability by formation of an SEI and an SL layer. Inspired by [132].

However, electrochemical impedance spectroscopy (EIS) is a viable *in situ* tool to monitor the SEI evolution with time **IV**, despite it does not provide information about its chemical composition. Studies performed by XPS combined with time of flight-secondary ion mass spectroscopy (TOF-SIMS) on fully lithiated or sodiated HC in 1 M LiClO₄ or NaClO₄ in propylene carbonate (PC), respectively, shown that despite the SEI formed on both electrodes contained similar compounds, their proportions was different [70]. The SEI compounds found in the SIB cell were mainly inorganic, *e.g.* Na₂O⁺, Na₂OH⁺, Na₂Cl⁺, while in LIBs the compounds were mainly organics, *e.g.* C₄H₃⁺, C₂H₅O₃⁺, C₂H₂O₅Li₃⁺ [70]. Moreover, the SEI formed on sodium metal electrode was found to be less stable than the one formed on a lithium metal electrode. The reason to the instability of the SEI could be due to the higher solubility of the Na-based electrolyte decomposition products in the solvents, as compared to Li-based compounds, as shown in [133] for 1 M MClO₄ (M= Li, Na) in PC. Despite many studies about the SEI in non-aqueous electrolytes of SIBs [7,69,70,134,135], up to date there are no investigations on the SEI formed in aqueous electrolytes or SPEs based sodium batteries.

PEO based electrolytes are less reactive toward sodium metal than water and organic liquid based electrolytes. Sodium, being a strong reducing agent, vigorously reacts with water, liberating heat and producing flammable hydrogen gas. The reactions between sodium and carbonate based electrolytes are more mild and result in decomposition products *e.g.* sodium carbonate (Na₂CO₃) and sodium formate (HCOONa) [136]. The stability of a Na[N(CF₃SO₂)₂] (NaTFSI) based SPE versus sodium metal has been evaluated in paper **IV**.

3.6 Ionic Conduction in Liquid and Polymer Electrolytes

Ionic conductivity (σ), is one of the most important parameter to evaluate an electrolyte for SIBs since poor Na^+ conduction can result in polarization issues which would lead to poor battery performance. The total ionic conductivity of an electrolyte can be defined as:

$$\sigma = \sum_i n_i \cdot |q_i| \cdot \mu_i \quad (1)$$

Where n_i is the number of charge carriers, q_i their charge and μ_i their mobility. From equation 1 it is intuitive that the conductivity will increase upon increase of charge carriers, commonly provided by the salts, their charge, and mobility. However, increasing the amount of charge carriers does not necessarily increase the σ of the electrolyte. Indeed, when increasing the concentration of Na^+ and anions, there will be an increase in their interaction which can lead to the formation of ion pairs (IP), contact (CIP) or solvent separated (SSIP), and aggregates.

In CIP, one or more solvent- Na^+ interactions are broken and replaced by one or more interactions with the anion. In SSIP the Na^+ is fully coordinated by the solvent but it is mutually attracted to the anion [137,138]. The IPs are neutral species which will not contribute to the conductivity, but to the mass transport [139,140]. Ionic aggregates are formed by the interactions of multiple ions. Moreover, due to the formation of aggregates, the viscosity of liquid electrolytes will also increase and, since mobility is inversely proportional to viscosity, as a result the conductivity will diminish. For PEO based electrolytes, the increase in salt concentration will give formation of inter-chain cross links between the Na^+ and the polymeric chains, which results in an increase of the T_g . As a result, above a certain salt content, the σ decreases with the salt concentration [57,98,141], **III** (Figure 9).

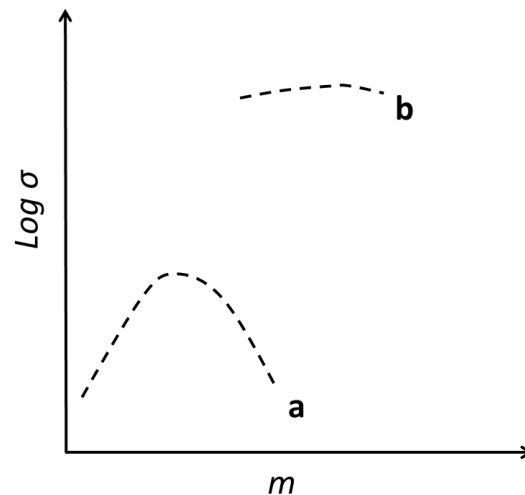


Figure 9. Schematic representation of the influence of the salt concentration on the σ for: a) SPE and b) LE. Inspired by [141] and [57], respectively.

However, the σ described in equation 1 is considerably higher than the Na^+ *partial* conductivity (σ_{Na^+}) since, often, most of the current is carried by the more mobile anions. This difference is especially important in ternary polymer electrolytes **V**, where the conductivity increase upon addition of IL is also due to the increase of ionic species. The σ_{Na^+} can be expressed as:

$$\sigma_{\text{Na}^+} = T_{\text{Na}^+} \cdot \sigma \quad (2)$$

T_{Na^+} represents the sodium transference number, defined as the fraction of current transferred by Na^+ , as free ions or in associated species. Several methods have been proposed for the determination of the transference number, mainly applied to lithium based electrolytes, and usually classified in electrochemical [142–145] or NMR based methods [101,142]. The σ_{Na^+} is usually $< 40\%$ of the σ , although there is not a standard method for the T_{Na^+} determination. The conductivities of most liquid (~ 1 M) and amorphous polymer electrolytes, above their T_g , plotted in an Arrhenius plot (Figure 10), show a curvature which follows the empirical VTF (Vogel-Tamman-Fulcher) [146–149] law:

$$\sigma = A \cdot T^{-\frac{1}{2}} \cdot e^{-\frac{B}{(T-T_0)}} \quad (3)$$

where A is a pre-exponential factor, proportional to charge carrier concentration and B the pseudo-activation energy. T_0 is the ideal glass transition temperature, which can be described in two different ways, following the two most common macroscopic models of ionic conductivity in SPEs. In the “free volume theory” [150] T_0 describes the temperature at which the available “free volume” is negligible. Whilst in the “configurational entropy model” [151] T_0 is the temperature at which the dynamic configurational entropy eventually reaches zero.

The σ of sodium based liquid and semi-crystalline polymer electrolytes, below their T_g , or in special crystalline SPEs [152,153] follows an Arrhenius law:

$$\sigma = \sigma_0 \cdot e^{-\frac{E_a}{RT}} \quad (4)$$

Where E_a is the activation energy associated with the ion transport, σ_0 is the conductivity when the temperature tends to infinity, and R is the gas constant. The conduction of the ions in such systems takes place through their hopping from one coordination site to another and the σ shows a linear behavior when plotted in an Arrhenius plot.

However, the presence of phase transformations, such as crystallization, which leads to formation of crystalline phases that hinder the ion conduction, can affect the shape of the typical “curved profile” **III**. Nonetheless, the conduction mechanism in the amorphous phase is unchanged. In Figure 11, an Arrhenius plot for the ionic conductivities of $\text{NaFSI}(\text{PEO})_9$ upon heating and cooling is shown. Only the cooling scan follows the VTF behavior and a hysteresis is observed between cooling and heating cycles. This is due to crystallization and subsequent melting phenomena that affects the shape of the conductivity plot **III**. A simple observation of the variation of macroscopic properties with temperature is not enough to

establish a conduction mechanism, but this must account for the material properties and here we can *e.g.* connect the SPEs with the dynamic percolation bond (DBP) theory, which will be described later.

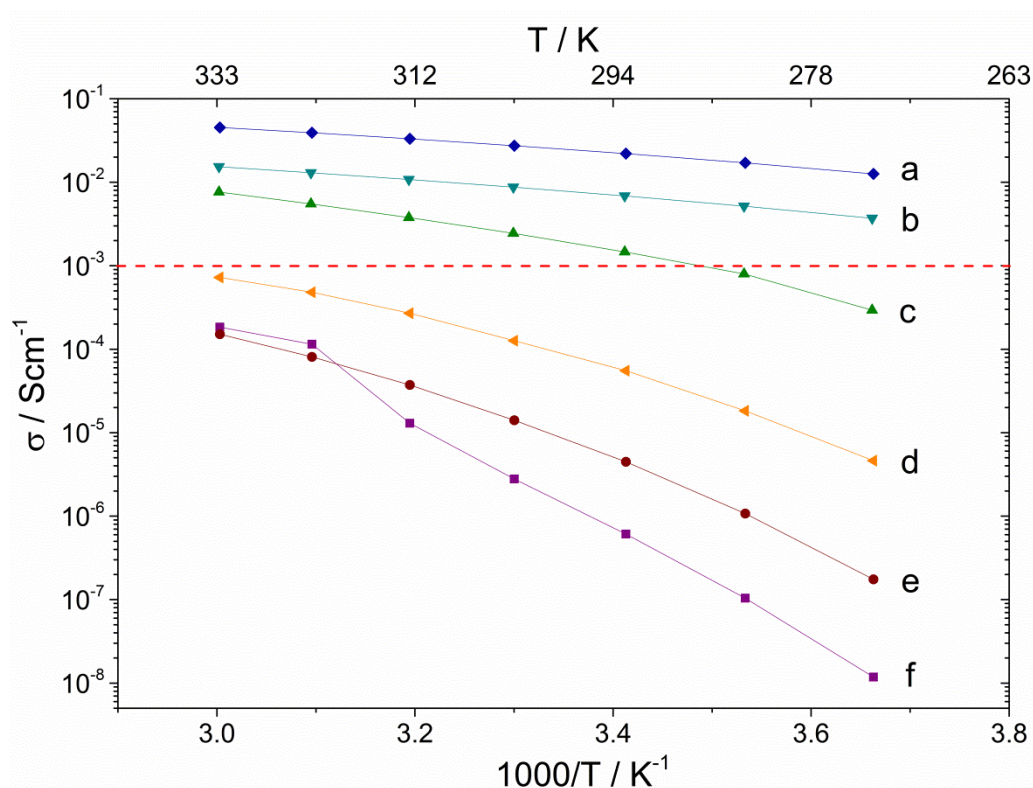


Figure 10. Arrhenius plots for selected liquid and solid sodium based electrolytes: a) 1.5 m NaMM441 in H₂O **II**, b) 0.8 m NaTFSI in EC-PC (1:1) [58], c) NaTFSI 0.8 m in Pyr₁₃TFSI [58], d) NaTFSI(PEO)₉ - 20 wt% Pyr₁₃TFSI **V**, e) NaTFSI(PEO)₉, and d) NaTFSI(PEO)₂₀ **III**.

In both liquid and PEO based electrolytes, the motion of the ions is coupled to the structural relaxation of the solvent. In electrolytes comprising Li⁺ and carbonate solvents, simulation studies has shown that the ion conduction takes place via two distinct mechanism: *vehicular* and *exchange with the solvent* [154], (Figure 12a and 12b). The *vehicular* mechanism consists in the motion of Na⁺, together with a solvent shell under the influence of an electric field. The *exchange with the solvent* mechanism describes a process in which the Na⁺ is exchanged between different solvent molecules. The contribution of the *exchange with the solvent* mechanism is higher than the *vehicular* mechanism in IL based electrolytes (Figure 12c and 12d), as observed by molecular dynamics simulation in Pyr₁₃TFSI doped with LiTFSI [155]. IL based electrolytes show lower σ than organic solvents and water based electrolytes mainly due to their higher η and high ionic association (Figure 10). σ of SPEs and ternary polymer electrolytes is lower than for liquid electrolytes (Figure 10) and still far from the 10⁻³ S cm⁻¹ (dashed line in Figure 10) [56]. Overall, the total ionic conductivity increases in the order:

$$\sigma_{\text{SPEs}} < \sigma_{\text{ternary polymer electrolytes}} < \sigma_{\text{ILs}} < \sigma_{\text{organic liquid}} < \sigma_{\text{aqueous}}$$

For polymer electrolytes, the σ usually decreases with the increase of the MW up to their entanglement limit [156]. Above this limit, the vehicular mechanism is no longer important [154,156], and the conduction mechanism is instead denoted as *segmental motion* (Figure 12e). The motion of ions in the amorphous phase of SPEs is coupled to the segmental motion of the polymer host, connected with locally changing configurations. The cation diffusion is a result of three types of motion: 1) intrachain motion along the polymer chain, 2) movement with the polymer chains and 3) interchain transfer between polymer chains [157]. Generally in SPEs, the ionic conduction takes place mainly in the amorphous phase [158] whereas conduction in the crystalline phase is only relevant for certain SPEs [152,153].

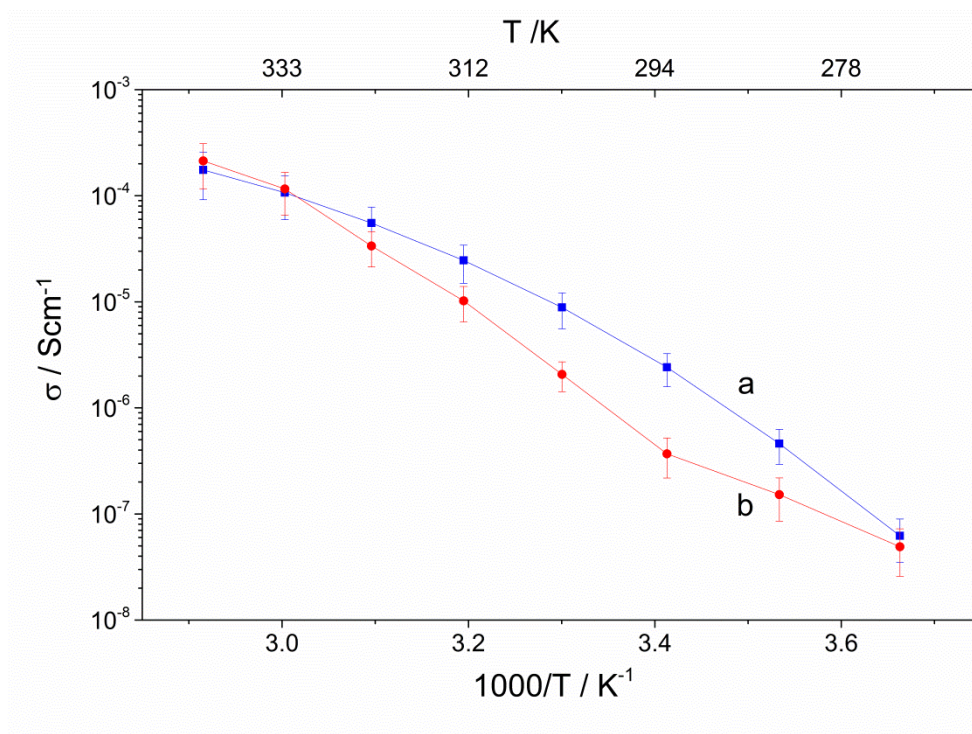


Figure 11. Arrhenius plot for NaFSI(PEO)₉ in the a) cooling and b) heating scan.

The DBP theory [158,159] gives a mechanistic insight into the conduction mechanism, in a *microscopic* to distinguish it from *macroscopic* approach, such as the VTF law. In PEO based SPEs, the ionic conduction takes place by the formation and breaking of Na⁺-O_{PEO} interactions and by additional movement of ions, hops between occupied and unoccupied sites. Since the Na⁺ conduction of PEO based SPEs is strongly coupled to the polymer dynamics, a common method to increase the σ of SPEs is to enhance the segmental dynamics, by decreasing their T_g via use of plasticizing ions **III**, **V**. In ternary systems **V**, the anions and Pyr₁₃ cation, which are only weakly solvated by the polymer, move faster in the locally created free space.

<i>Electrolyte</i>	<i>Vehicular</i>	<i>Solvent exchange</i>	<i>Segmental motion</i>
Organic liquid	Y	Y	N
Aqueous	Y	Y	N
IL	Y	Y	N
SPE ¹	N	N	Y

Table 4. Ionic conduction mechanisms of electrolytes.

Another strategy to increase the σ is to decouple the ion motion from the polymer dynamics, which cannot be done in small-molecule based electrolytes [160]. The decoupling of ion motion from the segmental motion of the polymeric chain can be obtained by using polymers with a relatively rigid backbone (high T_g) to obtain *superionic* polymer electrolytes [160–162]. However, in such electrolytes issues such as association (due to a low solvation of the polymer), result in conductivities that are still lower than in liquid electrolytes.

¹ Above its entanglement limit.

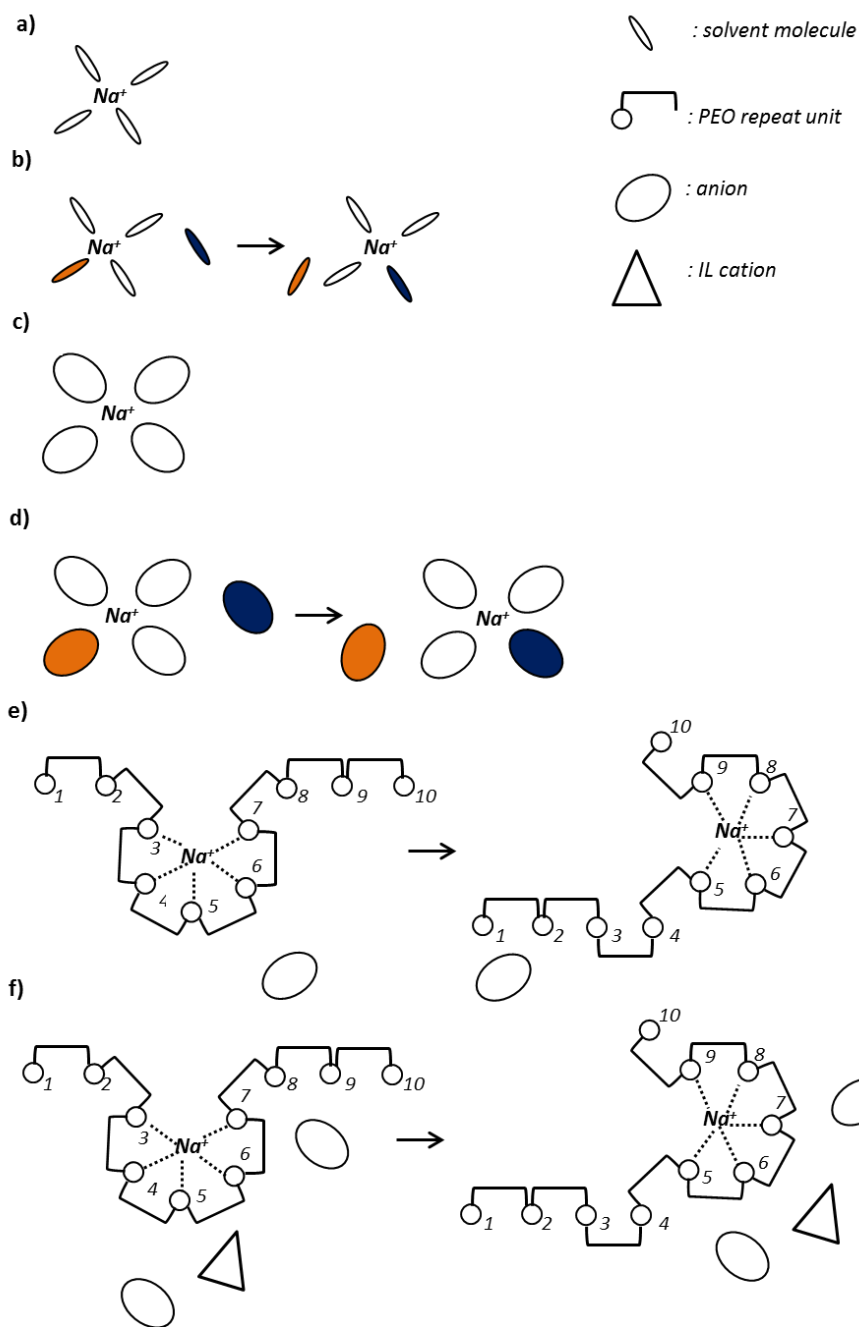


Figure 12. Simplified representation of the ionic conduction mechanisms in different electrolytes: a) vehicular in organic liquid based electrolytes, where the Na^+ moves together with the first solvation shell, b) solvent exchange in organic liquid based electrolytes, where the Na^+ conduction takes place with exchange of solvent molecules, c) vehicular in IL based electrolytes, d) exchange mechanism in IL based electrolytes, e) intrachain polymer segmental motion in SPEs, in which the Na^+ motion is coupled to the PEO dynamics, and f) intrachain polymer segmental motion in ternary polymer electrolytes.

4 Materials and Experimental Techniques

To assess the dynamics, the ionic speciation, and the compatibility of the electrolytes toward electrode materials are all crucial for the selection of a suitable battery electrolyte. In this section, the preparation of both sodium based liquid and polymer electrolytes as well as the basic principles of the techniques used for their characterization are introduced to assist in the understanding of the obtained results.

4.1 Preparation of Electrolytes

The preparation of non-aqueous electrolytes requires the use of dry solvents, including polymers and ionic liquids, and salts and their handling inside a glove box, in which an inert and dry environment is maintained (*e.g.* $O_2 < 5$ ppm, $H_2O < 1$ ppm). This is to avoid any water contamination which strongly affects electrolyte properties [163]. Liquid solvents are usually dried over molecular sieves, while polymers are heated under vacuum and different temperature, *e.g.* 50 °C for PEO. Salts are usually dried under vacuum (< 7 Pa) in conditions which depend on the salt's decomposition (T_d) and melting temperatures, (T_m), see 4.2. The drying conditions vary with the salts, *e.g.* $NaPF_6$ can be dried at 120 °C for 24h [57] while $NaTFSI$ is usually dried at 120 °C for 48 h **III**, [57].

For aqueous electrolytes these restrictions are of course not necessary, even though most salts need to be dried to avoid erroneous concentrations. Moreover, degassing of the aqueous electrolytes, through bubbling with an inert gas, *e.g.* Ar, N_2 , are necessary prior to electrochemical measurements, *e.g.* ESW determination (see 4.4).

In general, the electrolytes are prepared via mixing a suitable amount of a sodium salt with one or more solvents in order to obtain the desired composition. This process is straightforward for liquid electrolytes. For example, a 1:1 (v:v) blend of PC and EC is added to a certain amount of $NaPF_6$ and the obtained mixture is stirred. If necessary, the temperature can be increased to speed up the salt dissolution process. Despite preparing electrolytes based on molality (m) is more practical and avoids errors due to volume expansions, liquid electrolytes are most often prepared by molarity (M). Aqueous and non-aqueous liquid electrolytes commonly have a concentration of about 1 M **I**, [12,57,164]. This value was initially chosen to benchmark sodium based electrolytes with the commercial liquid electrolyte for LIBs (LP30) and proven to be close to optimal [69]. Recently, the concept of “water-in-salt” (~21 m) [83] and “super-concentrated” (~5 M) [165] electrolytes have become popular. The first concept was proposed to extend the ESW of aqueous electrolytes. “Super-concentrated” electrolytes [166,167] were introduced to replace the solvents commonly used in the electrolytes for commercial LIBs [165], and later shown to diminish the severe corrosion of the aluminum current collector, that usually takes place in PF_6^- free electrolytes [168], an outcome that can be relevant for SIBs as well.

The preparation of SPEs is considerably more demanding; a common method is to make a thin film, of about 20-200 μm thickness, by solvent casting. A polymer like PEO and a sodium salt (NaX), with the concentration given as the O/Na ratio, are first dissolved in a secondary solvent, *e.g.* acetonitrile, to obtain a homogeneous liquid solution. Then, the solution is casted in a PTFE mould, followed by evaporation of the secondary solvent. In

order to remove remaining secondary solvent residuals, the SPE is heated, *e.g.* to 50 °C, under vacuum [169]. For sake of comparison with liquid systems, the concentration of NaTFSI in NaTFSI(PEO)₉ is 2.5 m. A period up to several days is necessary for allowing “equilibration” *e.g.* the formation of crystalline phases, which improve the mechanical properties of the film, before the film is peeled off the mould and *e.g.* cut to discs. Since the morphology of the SPE depends on the casting method [170], a systematic procedure is crucial. The preparation of a polymer electrolyte through hot-pressing is an alternative to completely avoid the use of a secondary solvent [171–173]. In this method, the salt and the polymer are mixed, by ball milling or grinding in a mortar, together to obtain an intimate mixture which is later pressed between two metallic plates at > 100 °C. After cooling, an SPE film is obtained.

Ternary polymer electrolytes can also be prepared by solvent casting or hot-pressing. In the former case IL, sodium salt, PEO, and acetonitrile are mixed together and then casted in a PTFE mould **V**, while for hot-pressing, the three first components are mixed together, and annealed at ~100 °C to obtain an homogeneous rubber-like material and later pressed [174,175]. There is no standard content of IL, hence rather evaluated for every SPE and adjusted to the performance wanted. The addition of ILs to SPEs worsens the mechanical properties and above some IL contents the ternary electrolytes are difficult to handle since rubbery-like materials with adhesive properties are obtained. This can be partly circumvented by casting the electrolyte directly on the electrode material **V** or by improving the mechanical properties through cross-linking of the polymer [176].

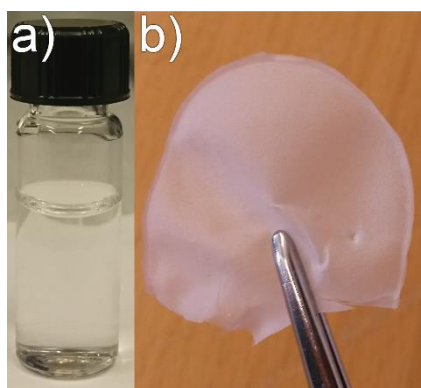


Figure 13. a) Liquid electrolyte and b) self-standing SPE film.

4.2 Thermal Analysis Methods

4.2.1 Differential Scanning Calorimetry

Calorimetry, *i.e.* the measurement of heat exchange, is a useful technique to detect the effects of thermal treatment on materials [177,178]. Many phenomena of electrolytes are related to a heat exchange, and calorimetry is particularly useful for detecting different phases in a SPE, crystallization in liquid electrolytes, as well as the glass transitions.

In heat flux differential scanning calorimetry (DSC) the heat difference between a sample and a reference, both subjected to the same thermal treatment, is measured. The sample (~10 mg) is placed in an aluminum pan and together with the reference, typically an empty aluminum pan that shows a known thermal behavior in the selected temperature window, heated or cooled at a certain rate (usually expressed in K/min) inside a furnace (Figure 14). Whenever an endothermic or exothermic process takes place, the temperature difference between sample and reference varies and is recorded by the thermocouples and the event can be detected.

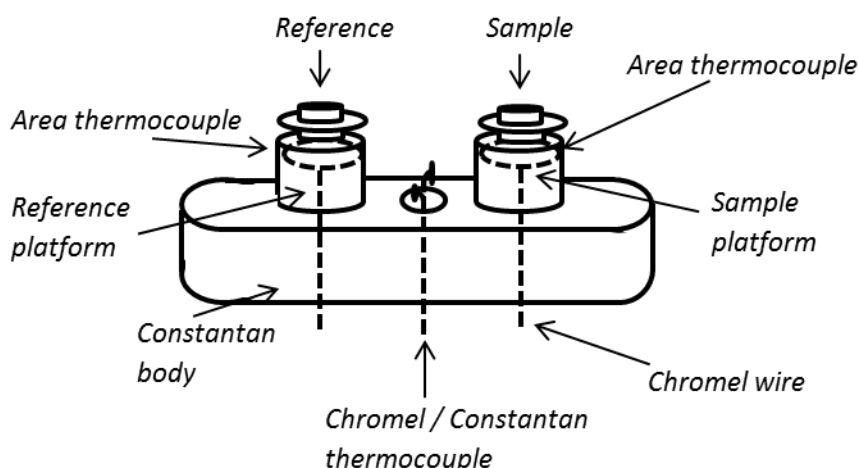


Figure 14. Schematic of a DSC furnace.

Liquid electrolytes are directly poured into the pan, while small pieces of SPEs are folded and attached to the bottom of the pan. In Figure 15, DSC heating traces registered at 10 K/min for the SPEs NaFSI(PEO)_n **III** are shown providing the main processes of glass transition, crystallization, and melting. The glass transition temperature (T_g) is observed as a variation in the slope of the baseline, while the crystallization (exothermic) and melting (endothermic) processes are obtained as peaks. The area underneath the melting peak gives the enthalpy of the melting process, which is proportional to the amount of SPE crystallinity. The 1st trace refers to the as prepared samples, with a larger amount of crystallinity than the 2nd trace. The T_g for $n:9$ increased after the 1st scan as the melting of crystalline phases allowed higher Na⁺ concentration in the amorphous domain, thus hampering the polymer chain dynamics. It is important to record the DSC traces both before and after melting to get hints on both crystallization kinetics and chain dynamics.

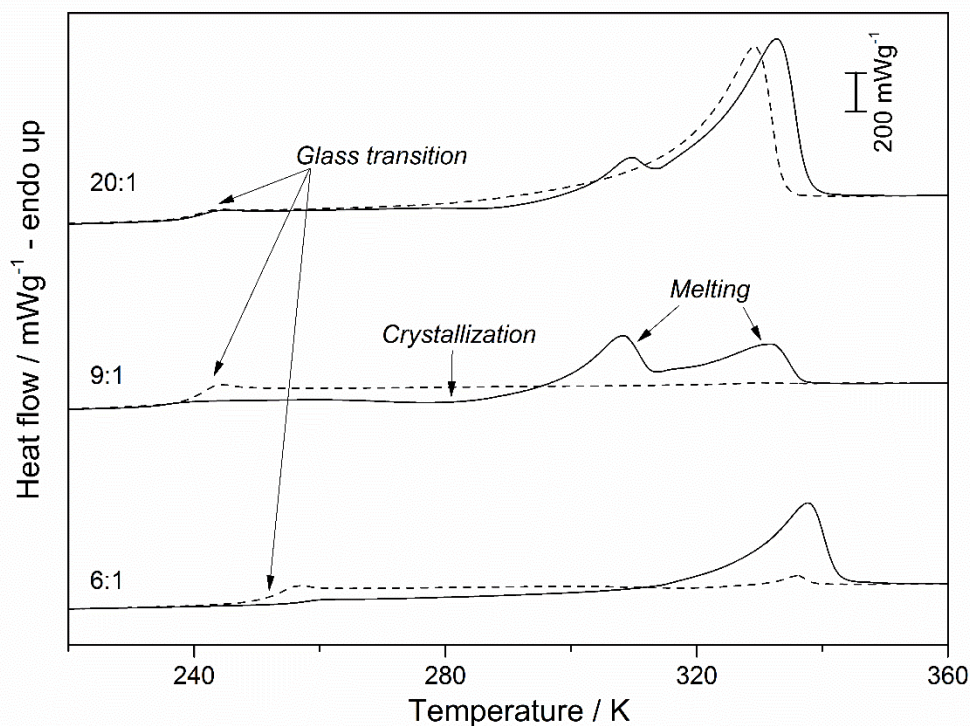


Figure 15. DSC heating traces for NaFSI(PEO)_n (*n*: 6, 9, 20). 1st scan (—), 2nd scan (---).

4.2.2 Thermal Gravimetric Analysis

The thermal stability of a chemical compound, *e.g.* useful when assessing the temperature at which a salt can be dried without decomposition, can be evaluated by monitoring its gravimetric variation upon heating, as in thermal gravimetric analysis (TGA) [179]. The sample (~10 mg) is commonly placed in a crucible, which can be made *e.g.* of aluminum (for $T < 600$ °C), platinum or alumina, located on a microbalance. During a measurement, gas (N₂ or Ar) is purged through the sample chamber to remove volatile decomposition products. A scheme of the TGA apparatus is displayed in Figure 16.

TGA experiments can be performed in a dynamic or isothermal mode. In the former, the sample is heated, usually to $T < 600$ °C II, [86,91], at a fixed rate to assess its thermal stability range. There is no standard scan rate, but lower heating rates give lower and stricter T_d , why it is recommended to perform all measurements at the same scan rate, *e.g.* 5 °C min⁻¹. In the isothermal mode, the sample is kept at a fixed temperature over a period of time, to acquire information on long term stability. In this work, only dynamic mode was adopted.

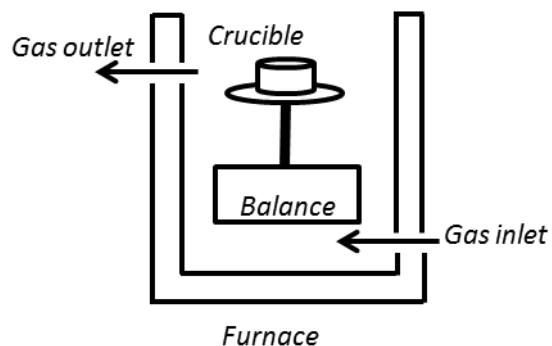


Figure 16. Schematic of a TGA apparatus.

A typical dynamic TGA heating trace shows the gravimetric loss, expressed in wt%, as a function of temperature as depicted in Figure 17. Thermal stability is usually evaluated by the T_d , which can be estimated by different methods. The temperature corresponding to the % of weight loss upon heating, *e.g.* $T_{1\%}$, is usually more stringent than the extrapolated onset temperature (T_{onset}) obtained from the intersection of the slope of weight loss process and the horizontal 0 % weight loss (Figure 17).

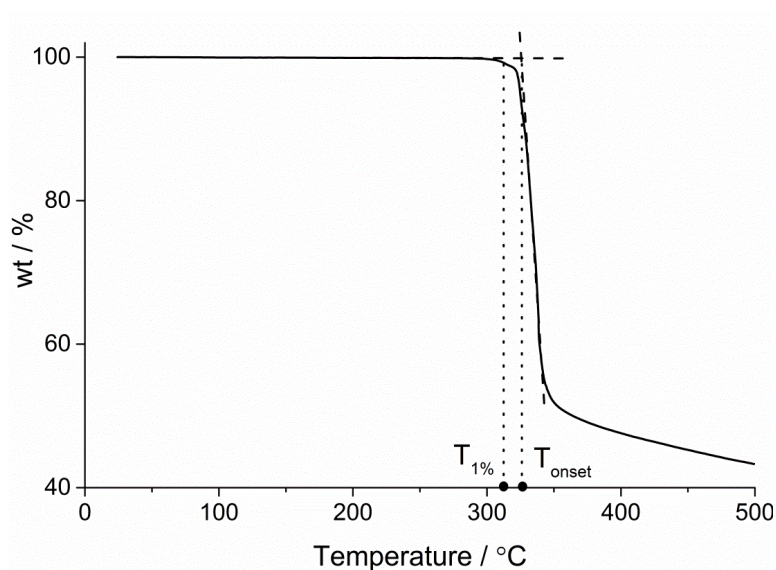


Figure 17. Typical TGA plot with the graphical determination of $T_{1\%}$ and T_{onset} shown.

4.3 Vibrational Spectroscopy

4.3.1 Raman Spectroscopy

Raman vibrational spectroscopy is based on the inelastic scattering that takes place when radiation of suitable wavelength hits a material [180]. When monochromatic radiation interacts it induces a distortion of the electron cloud as a result of which an electric dipole moment P is induced and defined as:

$$P = \alpha E \quad (5)$$

where α is the polarizability of the material and E is the electric field of the radiation.

A photon interacts with a molecule exchanging energy (and momentum), leaving it with an energy that can be higher (anti-Stokes) or lower (Stokes) than its initial one (Figure 18). The phenomenon can be simply described as excitation or de-excitation of a “virtual state” as depicted schematically in Figure 18. Stokes transitions are usually preferred as the probability is higher and therefore a better signal to noise ratio is obtained. Since the Raman cross section is very low, competing phenomena such as fluorescence should be avoided *e.g.* by adopting a less energetic laser beam such as the 1064 nm line of a Nd:YAG laser.

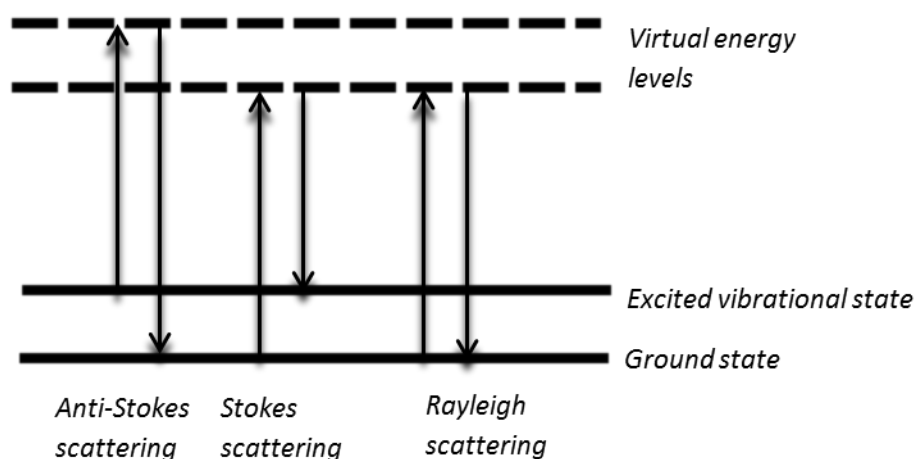


Figure 18. Schematic of the Raman effect. Rayleigh scattering is shown for comparison. Inspired by [181].

Liquid electrolytes are simply placed in a properly sealed glass vial, while for a SPE a stripe of film is folded and placed on the surface of a glass vial. Raman spectroscopy is a useful technique for information about ionic speciation *e.g.* the presence of contact ion pairs or aggregates in SPEs can be detected. Indeed, examining the vibrational modes of the anions, for example TFSI and FSI, and their shifts it is possible to evaluate the interaction with Na^+ . In Figure 19, the Raman spectra in the range $700\text{-}770\text{ cm}^{-1}$ are given for $\text{NaFSI}(\text{PEO})_n$.

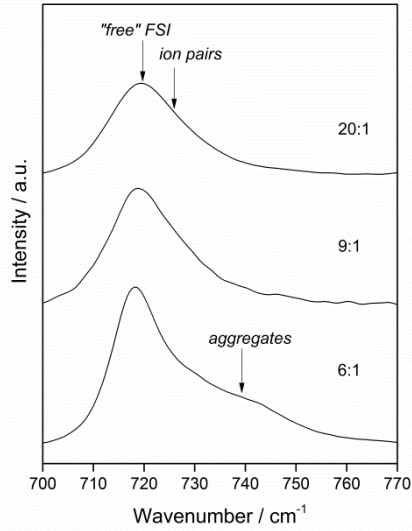


Figure 19. Raman spectra for NaFSI(PEO)_n (n: 6, 9, 20) in the range 700-770 cm⁻¹. The arrows indicate bands of “free” FSI, ion pairs and aggregates.

The bands depicted in Figure 19 are composed of an overlapping of individual bands and in order to resolve them, a curve fitting is performed [182]. The fitting procedure consists in simulating the band registered experimentally with a set of individual bands, which are described with a mathematical function. The Gaussian and Lorentzian profile usually account for inhomogeneous and homogeneous broadening, respectively. The convolution of the two functions gives a Voigt profile.

In **III**, a quantitative determination of the amount of free anions and SSIP, CIP, and aggregates for NaTFSI(PEO)_n and NaFSI(PEO)_n was carried out. For NaTFSI(PEO)₉ (Figure 20), the band corresponding to the expansion-contraction mode of the TFSI anion [183] was simulated with two bands. The first band, located at 740 cm⁻¹ was simulated with a Voigt function (equation 6) and assigned to the “free” TFSI anion and to SSIP.

$$V(x) = \frac{a_0}{\sqrt{\pi} \cdot a_2} \cdot \int_{-\infty}^{\infty} \frac{e^{-t^2}}{a_3^2 + \left(\frac{x - a_1}{a_2} - t\right)^2} dt \quad (6)$$

Where a_0 is the amplitude, a_2 is the width and a_3 is proportional to the ratio of Lorentzian and Gaussian widths. The second band, located at 744 cm⁻¹ (Figure 20), was assigned to CIP and simulated with a Gaussian function (equation 7).

$$G(x) = \frac{a_0}{\sqrt{2\pi} \cdot a_2} \cdot e^{\left[-\frac{1}{2} \left(\frac{x - a_1}{a_2}\right)^2\right]} \quad (7)$$

Where a_0 is the area, a_1 is the center and a_2 is the width.

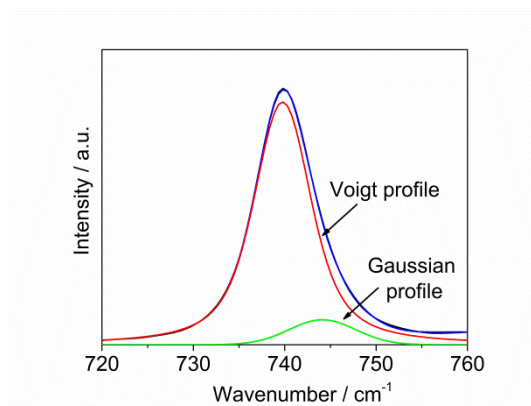


Figure 20. Fitting of the band assigned to the expansion-contraction mode of the TFSI anion in NaTFSI(PEO)₉. The Voigt profile and the Gaussian profile were used to fit the "free" TFSI anion and the CIPs, respectively.

Moreover, others bands are useful to determine the presence of strong interactions between the polymer chains and the cations (Figure 21). Here, when Na⁺ interacts with PEO, a new band appears at about 863 cm⁻¹, due to a created collective breathing mode of several polyether segments [184]. Moreover, the band at *ca.* 844 cm⁻¹ (Figure 21), usually assigned to crystalline PEO [185], disappears when going from n=20 to n=9,6, due to an increase of the amorphous phase content.

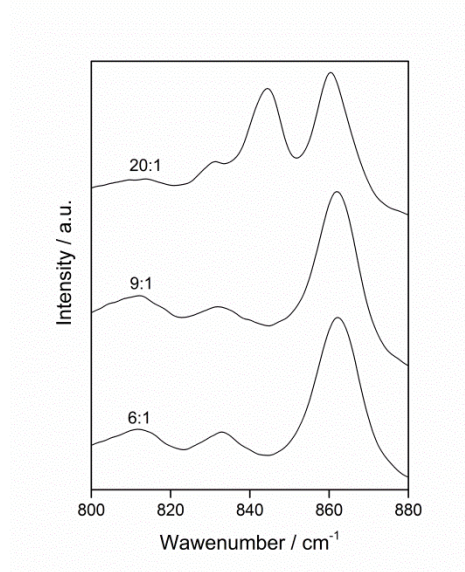


Figure 21. Raman spectra for NaTFSI(PEO)_n (n: 6, 9, 20) in the range 800-880 cm⁻¹.

4.3.2. Infrared Spectroscopy

Infrared (IR) vibrational spectroscopy is based on the excitation, of the vibrational states of chemical bonds of a material through incident far-IR or mid-IR radiation: $10\text{-}400\text{ cm}^{-1}$ and $400\text{-}4000\text{ cm}^{-1}$, respectively [186]. In an IR spectrometer, using a transmission set-up, the sample is exposed to a polychromatic IR radiation. Photons are adsorbed when their energy ($h\nu$) equals the energy difference between the vibrational ground state and the excited state but only if this induces a variation of the dipole moment of the molecule. IR spectroscopy can provide valuable and complementary information to Raman spectroscopy, since some vibration modes can give weak or no bands in Raman, but strong bands in IR, and *vice versa*.



Figure 22. Schematic of IR photon absorption.

Attenuated total reflectance (ATR or ATR-IR) spectroscopy is a sampling technique that allows measurements on liquids and solids in a simpler way than transmission IR *e.g.* sample preparation and reproducibility. The sample is placed on a reflective element of high refractive index (n_1), *e.g.* diamond, an IR beam is reflected from the surface and creates an evanescent wave, penetrating the sample with refractive index n_2 at a depth between $0.5\text{-}3\text{ }\mu\text{m}$, depending on the conditions (Figure 23). The evanescent wave is partly absorbed by the sample, resulting in decreased intensities at certain wavenumbers, and a spectrum is generated by signal processing of the reflected beam.

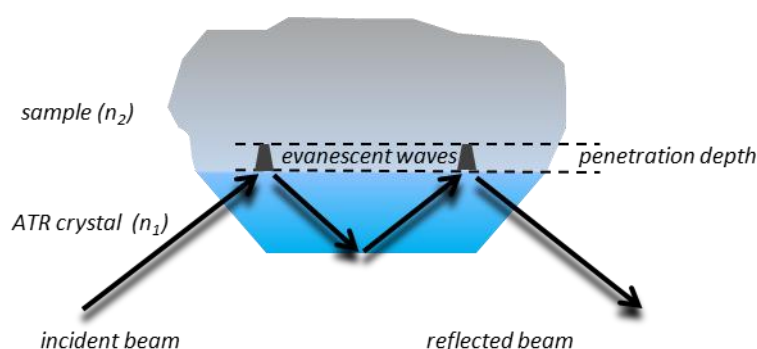


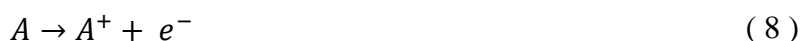
Figure 23. ATR working principle.

4.4 Electrochemical Methods

4.4.1 Potentiodynamic Methods

In potentiodynamic methods a direct current (DC) potential sweep is applied to a working electrode (WE), and the resulting current flowing between the WE and an auxiliary (counter) electrode (CE) is registered. The potential is usually referred to a suitable reference electrode (RE) through which no current passes. All three electrodes are always in contact with the electrolyte, but the cell configuration differs for liquid and solid electrolytes. A standard Swagelok three-electrode type cell [187] is commonly used for liquid electrolytes, while for polymer electrolytes different set-ups are preferred and an example is given in **IV**.

The plot of the current as a function of the potential is known as voltammogram and provides information on the kinetics of the charge transfer (CT), a faradaic process taking place at the WE. In a system comprising an electrochemical active species A a background current can be registered due to non-faradaic processes, at potentials where no charge transfer is taking place, associated with double layer effects (Figure 24.i). When the potential is swept toward more positive values, an oxidation process, involving the species A, can take place and a positive current is registered (Figure 24.ii):



When the potential is swept towards a more negative potential, a reduction process of the oxidized species A^+ can occur and a negative current is registered (Figure 24.iii):



If the CT is limited by the diffusion of the electroactive species, a peak related to the CT can be detected. The potential sweep can be performed in one direction toward reducing or oxidizing potentials, linear sweep voltammetry (LSV), or can be reversed at a predefined potential, cyclic voltammetry (CV). LSV can be useful for estimating the ESW of an electrolyte, while CV is used to study the properties of electrochemical species *e.g.* the potential at which the decamethyl ferrocene couple, $Me_{10}Fc^{+/0}$, is at in $NaTFSI(PEO)_9$ (Figure 24). In Figure 24, two peaks are shown: the anodic peak, E_{pa} ($Me_{10}Fc^0 \rightarrow Me_{10}Fc^+ + e^-$) and the cathodic peak, E_{pc} ($Me_{10}Fc^+ + e^- \rightarrow Me_{10}Fc^0$). For a one-electron reversible reaction a potential difference of 59 mV between E_{pa} and E_{pc} should be obtained and the obtained difference of ~85 mV can be due to uncompensated resistance and/or a quasi-reversible behavior **IV**.

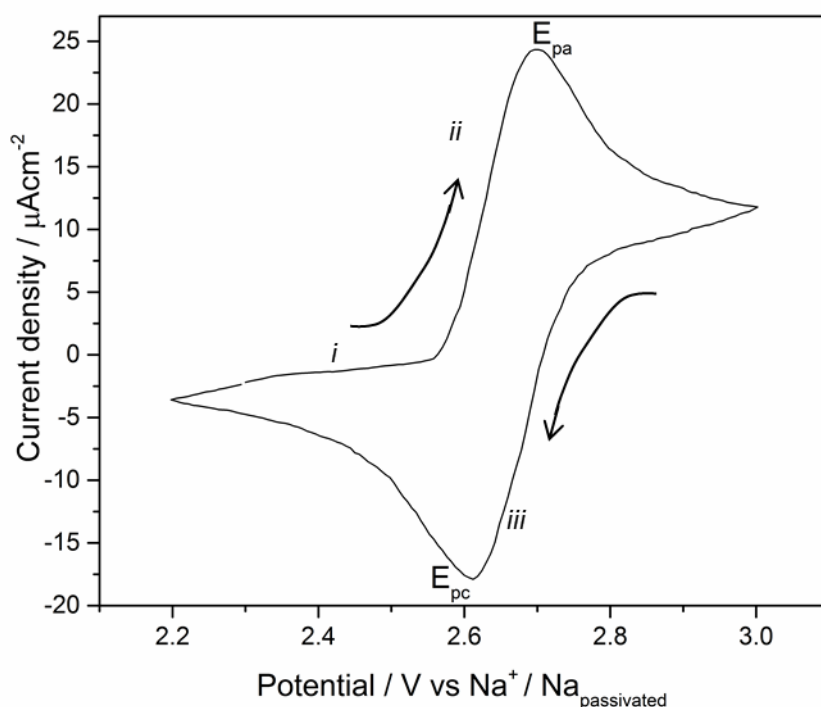


Figure 24. CV for the $\text{Me}_{10}\text{Fc}^{+/0}$ couple (~ 5 mM) in $\text{NaTFSI}(\text{PEO})_9$ registered at 20 mVs^{-1} on a Pt disc. A Na metal ring was used as RE.

4.4.2 Alternating Current Techniques

Alternating current (AC) techniques are useful tools for evaluating the response of electrochemical systems to a sinusoidal stimulus and are often employed to evaluate the σ of electrolytes **II**, **III**, **V** and to study the interface electrode/electrolyte **V**. Indeed, DC methods can give rise to polarization issues when, *e.g.* measuring the conductivity of electrolytes.

A voltage sine wave can be defined with the following equation:

$$E = E_0 \sin(\omega t) \quad (10)$$

where E_0 is the amplitude of the signal, t is the time and ω is the angular frequency, $\omega = 2\pi\nu$, ν is the frequency.

When a voltage sine wave is applied to an electrical circuit, the resultant current can be expressed as the following:

$$I = I_0 \sin(\omega t + \vartheta) \quad (11)$$

where ϑ represents the phase shift between the two signals. The applied sinusoidal voltage across a circuit and its response can be depicted in Figure 25.

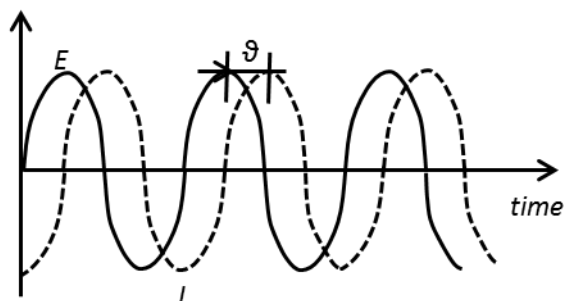


Figure 25. Phase shift between a sinusoidal voltage and its response current.

In AC regime, the ratio between the voltage across an element of an electrical circuit and the current flow is defined as its impedance which can be defined using complex numbers:

$$Z = Z_r + jZ_j \quad (12)$$

Where Z_r represents the real part of the impedance, a resistance as defined with the Ohm's law in DC regime. Z_j represents the frequency dependent part of the impedance, the reactive impedance, typical of ideal capacitors and inductors.

Electrochemical impedance spectroscopy (EIS) and dielectric spectroscopy (DS) are techniques that allows the characterization of electrochemical systems by applying a sinusoidal voltage (E usually 5-10 mV) and measuring its current response over a range of frequencies. I_0 and ϑ are analyzed by the Fourier transform of $I(t)$ and $E(t)$ and hence the impedance can be evaluated. For more about the mathematical treatment of the impedance, the following books are suggested [188–190].

The impedance measurement is performed with an impedance analyzer that can be coupled to a dielectric analyzer to evaluate the dielectric properties of a material [191,192]. The data can be represented graphically in a complex plane plot, referred as Argand or Nyquist plot [188–190], which is obtained representing, for each frequency, the real and imaginary part of the impedance (Figure 26).

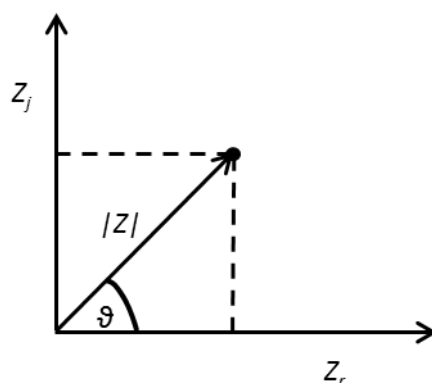


Figure 26. Impedance plot, for a fixed frequency, in the complex plane. $|Z|$ and ϑ are the module and the phase of the impedance, respectively.

Interpretation of impedance data is usually made by simulation with different equivalent circuits (ECs) [188–190], wherein each element, resistor, capacitor, *etc.* describes a specific physical phenomenon *e.g.* migration of ions, charge transfer, double layer, *etc.* ECs can be used to obtain the conductivity of an electrolyte and for analyzing the interfaces between electrolytes and electrodes.

4.4.2.1 Ionic Conductivity of Electrolytes

The ionic conductivity of electrolytes is usually obtained by measuring the impedance of a cell comprising the electrolyte between two blocking electrodes², *e.g.* stainless steel discs. A liquid electrolyte can be placed in a PTFE ring spacer, while a SPE film is often directly inserted between the two electrodes. The conductivity is usually evaluated at different temperatures and an equilibration time, *e.g.* half an hour, is necessary to guarantee the same temperature throughout the sample. To assure a good electrolyte-electrode contact, the cell containing a SPE can first be heated at temperatures $> T_m$ **III, V**.

The equivalent circuit in Figure 27 simulates the response of an ideal cell comprising blocking electrodes [193].

² An electrode is defined as non-blocking or blocking if, under the measurement conditions, a charge transfer with the electrolyte does or does not take place, respectively.

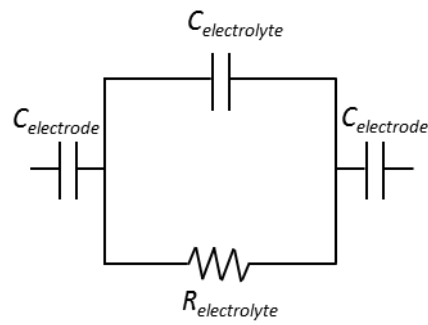


Figure 27. Scheme of an EC used to simulate a cell with blocking electrodes (inspired by [193]).

This circuit is comprised of the capacitance of the blocking electrodes ($C_{\text{electrode}}$) and the electrolyte ($C_{\text{electrolyte}}$), and the electrolyte resistance ($R_{\text{electrolyte}}$), which can give the following response, depicted in Figure 28, when plotted in a Nyquist plot:

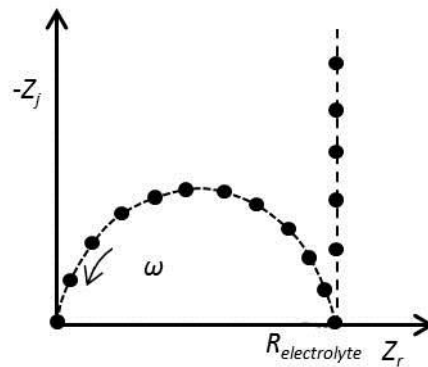


Figure 28. Simulated impedance from the EC depicted in Figure 27 (inspired by [193]).

For real systems, a constant phase element (CPE) [188–190] can be used in place of the capacitors (Figure 27) for accounting the non-ideal electrolytes [193] and electrodes [194]. A typical impedance response for a SPE is depicted in Figure 29.

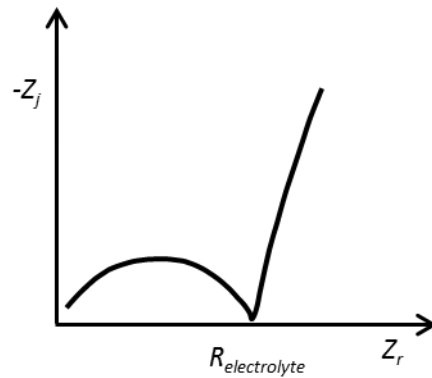


Figure 29. Impedance response for a SPE / blocking electrode cell.

For liquid electrolytes above specific temperatures, the Nyquist plot of the impedance does not give a semicircle as in Figure 29 but rather a tilted line. The intercept of this line with the x-axis, at high ν , is the $R_{\text{electrolyte}}$. This is due to the higher ionic conductivity of liquid electrolytes, compared to SPEs, which correspond to faster processes that take place at higher frequencies.

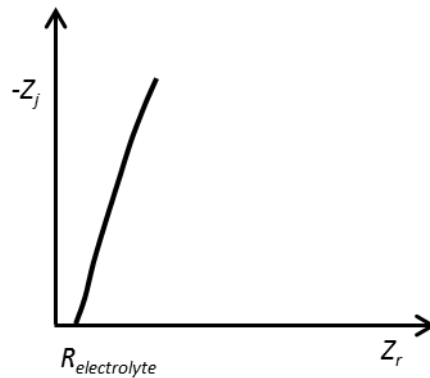


Figure 30. Impedance response for a liquid electrolyte / blocking electrode cell.

For a cell comprising disc electrodes, the ionic conductivity can be obtained by:

$$\sigma = \frac{4 \cdot s}{d^2 \cdot \pi \cdot R_{\text{electrolyte}}} \quad (13)$$

Where, s is the thickness of the electrolyte (SPEs) or the spacer thickness (liquid electrolytes), d is the diameter of the electrodes (SPEs) or the inner diameter of the spacer (liquid electrolytes). $R_{\text{electrolyte}}$ is the resistance of the electrolyte, as obtained from the Nyquist plots depicted in Figure 29 and Figure 30. However, the method described assesses the *total* ionic conductivity of the electrolytes, due to the all ionic species (Na^+ , anions, aggregates, *etc.*).

4.4.2.2 Evaluation of the Interface Electrode / Electrolyte

EIS can be used to evaluate the interface between a sodium based electrolyte and a non-blocking electrodes, such as Na metal. When the measurement is performed in a three-electrode cell **IV**, the resistance of the interface between the Na metal, WE, and the electrolyte, $R_{Na/SPE}$ can be obtained (Figure 31). Moreover, as sodium is a very reactive metal it will most likely oxidize in contact with the electrolyte and the stability of this passivation layer can be evaluated *e.g.* monitoring its impedance.

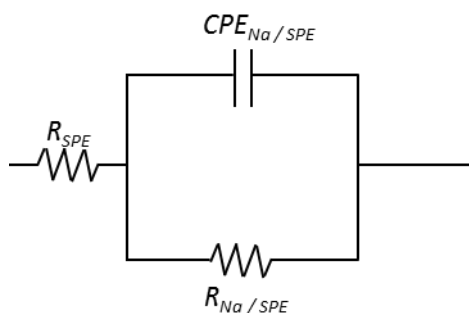


Figure 31. Equivalent circuit used for analyzing the impedance data for a three-electrode cell comprising sodium metal as WE and NaTFSI(PEO)₉ as electrolyte **IV**.

4.4.3 Karl Fischer Coulometric Titration

Water is commonly known to have a large effect on the properties of electrolytes and is therefore crucial to assess the water content for all non-aqueous electrolytes. The most common determination method is Karl Fischer (KF) titration [195,196], based on the reaction between iodine and the water present - the KF reaction [197].

The KF titration can use a coulometer [198], where the iodine is produced electrochemically and, if water is present, a current will be registered until the end point is reached [199]. A drawback is that due to the detection limits a minimum amount of water must be present to obtain reliable results and hence for samples with low concentration of water, 10-20 ppm, a considerable amount of sample is needed. For liquid electrolytes these are injected into the KF coulometer, while for SPEs the analysis can be performed in two different ways:

1. The SPE is dissolved in a suitable dry solvent *e.g.* acetonitrile and then injected in the KF reagents.
2. The SPE is heated in an oven to remove water, which then is conveyed in the KF apparatus.

In order to determine the water content in the PEO based SPEs and in the ternary electrolytes **III** - **V** the first method was used; simpler and no dedicated oven is required.

5 Summary of appended papers

Paper I

Non-aqueous electrolytes for sodium-ion batteries

In this review paper, we provide an overview of electrolytes that have been used in sodium-ion batteries (SIBs). SIBs represent a viable and sustainable alternative to the well-established lithium-ion batteries (LIBs). The electrolyte in its basic form comprises of a sodium salt dissolved in a solvent and the fast-growing research on SIBs focuses on both components. Due to the similarities between Li^+ and Na^+ , the sodium salts are usually the sodium version of salt used in LIBs. From an overview of the liquid and solid solvents we find that they are not necessarily the same as those employed in LIBs since other factors play a role, *e.g.* the compatibility with electrodes. A liquid electrolyte comprising carbonates and NaPF_6 is the first choice, due to the performance in term of ionic conductivities, electrochemical stability window, compatibility with the electrodes, *etc.* However, every combination of salts and solvents shows interplay of pros and cons. The organic based electrolyte for example still keeps the same flammability concerns as in LIBs. Ionic liquids have large promises since they have lower flammability hazards than carbonate based electrolytes but still do not represent a viable candidate. Alternatives could be solid polymer electrolytes but yet the lower ionic conductivity still hinders its use for room temperature (RT) applications.

Calculated natural capital cost [€ per kW h capacity]				
	SIBs		LIBs	
Elem.	HC elec ^a NVPF	C ₆ LP30 LFP	C ₆ LP30 LMO	LTO LP30 LMO
Al	0.36	0.18	0.11	0.51
C	0.073	0.08	0.057	0.068
Cu	—	185	110	—
F	2.17	1.09	0.8	2.42
H	0	0	0	0
Fe	—	0.6	—	—
Li	—	0.0085	0.0078	0.04
Mn	—	—	6.56	15.1
O	0	0	0	0
P	1.43	0.15	0.081	0.24
Na	0	—	—	—
Ti	—	—	—	1.56
V	27.5	—	—	—
Sum	31.5	187	117	19.9

^a 1 M NaPF_6 in EC:PC:DMC HC = hard carbon, NVPF = $\text{Na}_3\text{V}_2(\text{PO}_4)_2\text{F}_3$, C₆ = graphite, LP30 = LIB standard electrolyte, LFP = LiFePO_4 , and LMO = LiMn_2O_4 .

Figure 32. Calculated capital costs for different LIBs and SIBs. Reproduced from I with permission from the Royal Society of Chemistry.

Paper II

Fluorine-free salts for aqueous lithium-ion and sodium-ion battery electrolytes

State-of-the art SIBs and LIBs contain a combination of organic liquid solvents and fluorine based salt. However, both the solvent and the salt show safety issues and upon decomposition the electrolyte releases toxic gases. Moreover, the production of fluorine-based compounds is dangerous and expensive. When it comes to the salt, most of the concerns arise from the anion, this is why the SIBs and LIBs research aims to develop next generation-anions which are fluorine-free. In this work, a first generation of sodium and lithium based fluorine-free salts which contain the Mickey MouseTM (MM) anion, is characterized by different techniques. In these salts, NaMM4411 and LiMM4411, the negative charge is not localized in specific regions of the molecule, but is pseudo-localized. These salts have problems that need to be addressed, i.e. the limited solubility in organic liquids solvents and in PEO. Indeed, the MM based salts show strong interactions between the Na⁺ or Li⁺ with the negative SO₃⁻ groups, probed by IR and Raman spectroscopy. However, the NaMM4411 and LiMM4411 salts are soluble in water and their electrolytes show conductivities comparable to LiTFSI based aqueous electrolytes. Moreover, the electrochemical stability window (ESW) of the MM based salts is comparable with aqueous electrolytes containing inorganic anions such as NO₃⁻ or SO₄²⁻. These outcomes open up for applications of the first generation of MM salts in low voltage aqueous SIBs and LIBs.

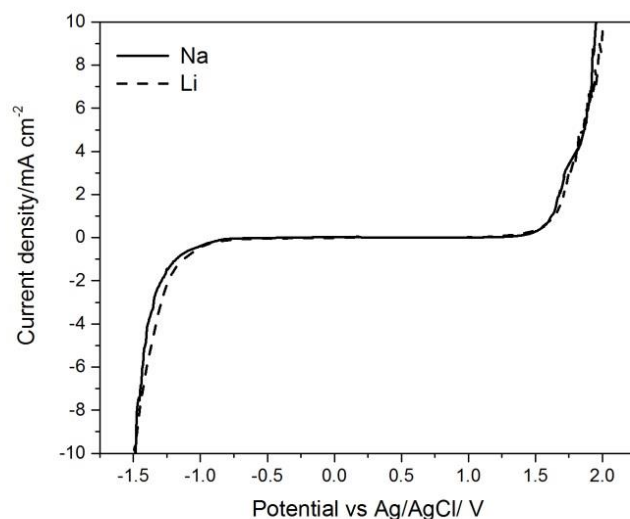


Figure 33. ESW for NaMM4411 and LiMM4411 based aqueous electrolytes. Reproduced from **II** with permission from the Royal Society of Chemistry.

Paper III

Characterization of NaX (X: TFSI, FSI) - PEO based solid polymer electrolytes for sodium batteries

In this work, NaFSI(PEO)_n and NaTFSI(PEO)_n solid polymer electrolytes (SPEs) are in focus. NaFSI is chosen with the aim to improve the dynamics of the PEO and thus the SPE conductivity. NaFSI based SPEs are then compared with the analogous electrolytes comprising the TFSI anion, one of the most used ions in SPEs. In both NaTFSI(PEO)_n and NaFSI(PEO)_n no salt precipitation is detected. It is confirmed that the TFSI anion inhibits crystallization, as proposed for the Li based SPEs while, for the first time, it has been observed that the FSI anion promotes PEO crystallization for $n=6$ and 9. This phenomenon is the reason of the presence of a pronounced hysteresis between cooling and heating scans that dramatically affects the conductivity of NaFSI(PEO)₉ and NaFSI(PEO)₆. The T_g of both TFSI and FSI based SPEs decrease with n as shown previously also for the analogous PEO based SPEs. For $n=20$ and 9 the FSI ion seems to be equally plasticizing as the TFSI ion, but for $n=6$ the different speciation in terms of charge carriers also affects the relative dynamics of the polymer chains. Indeed, for NaFSI(PEO)₆, presence of aggregates is detected, with Raman spectroscopy, contrary to the analogous TFSI based systems. Overall, FSI based SPEs show lower room temperature (RT) conductivities than the TFSI analogues. From a practical, battery oriented perspective, NaTFSI(PEO)₉ shows the better total performance but yet the total ionic conductivity is still lower than 10^{-3} S cm⁻¹ at RT.

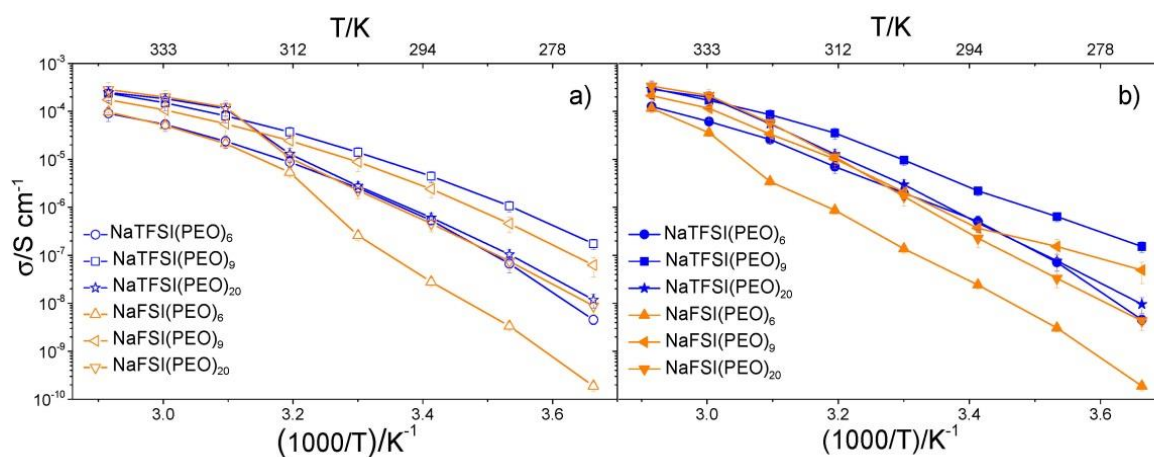


Figure 34. Arrhenius plots for NaTFSI(PEO)_n and NaFSI(PEO)_n with $n=6, 9,$ and 20 . a) cooling and b) heating scans. Reproduced from **III**.

Paper IV

On the feasibility of sodium metal as pseudo-reference electrode in solid state electrochemical cells

In this manuscript we evaluate the feasibility of sodium metal as pseudo-reference electrode (pseudo-RE) in half cell configuration comprising NaTFSI(PEO)₉ as electrolyte. Half-cell tests on SIB materials, often comprise the use of a working electrode (WE), counter electrode (CE) and metallic sodium as pseudo-RE. A suitable pseudo-RE should show a stable and reproducible potential when tested in the same electrolyte. However, sodium is highly reactive towards impurities such as water and oxygen and toward common organic liquid solvents. Moreover, sodium decomposition products were proven to affect by cross-contamination the performance of the WE. PEO based SPEs are stable versus lithium metal and similarly it can be inferred that they should mitigate the sodium corrosion. However, we show that sodium is not suitable as pseudo-RE in NaTFSI based SPE. Indeed, sodium metal cannot guarantee a stable and reproducible potential, as evaluated with impedance spectroscopy (EIS), open circuit voltage (OCV) measurements, and by monitoring the half wave potential $E_{1/2}$ of a standard redox couple as decamethyl ferrocene (Me_{10}Fc). This is mainly due to the reaction of the metal with the SPE, and to the reaction of sodium with impurities during the assembling of the cell as we show with ATR-IR spectroscopy. These findings call for attention when using sodium metal as pseudo-RE for the tests of SIBs materials and shed a light on the need of suitable REs for SIBs.

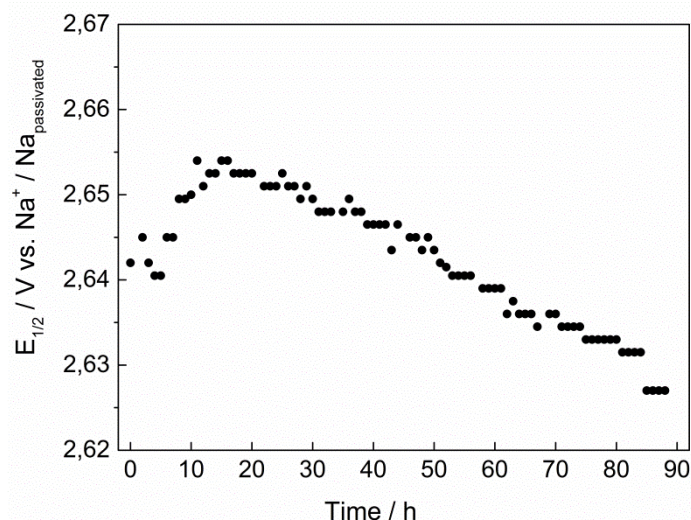


Figure 35. Half-wave potential of the $\text{Me}_{10}\text{Fc}^{+/-}$ redox couple in NaTFSI(PEO)₉.

Paper V

Plasticization of NaX-PEO by Pyr₁₃ ionic liquids

The addition of ILs to Li based SPE has proven beneficial in order to improve the polymer dynamics and the ionic conductivity at room temperature (RT) of PEO based SPEs. However, in most cases the IL addition is quite significant (up to 50 wt%) and to guarantee suitable mechanical properties, the PEO often needs to be cross-linked. In this paper we investigate the effect of moderate addition (<20 wt%) of Pyr₁₃ based ILs on the ionic speciation, polymer dynamics and total ionic conductivity of NaTFSI(PEO)_n and NaFSI(PEO)_n SPEs, with *n*: 6, 9, 20. The addition of ILs increases the polymer dynamics, exhibiting a plasticizing effect. The total ionic conductivity increases due to a combination of increased ionic species and improved polymer dynamics. Moreover, the addition of ILs is beneficial to suppress the PEO crystallization that took place in the FSI based binary systems. However, the ion association seems to be not affected by moderate addition of anions (TFSI or FSI) and Pyr₁₃ cation. Our results show that the Na⁺ conduction mechanism is not strongly affected by the presence of the ILs' anions and cations as they interact only weakly with the PEO. The conduction mechanism in such ternary polymer electrolytes is then similar to that taking place in the native SPEs.

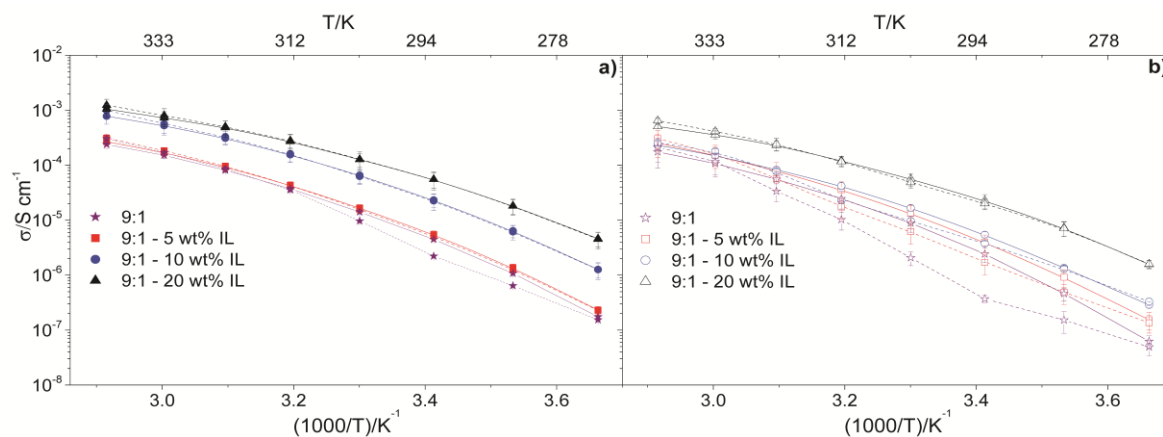


Figure 36. Arrhenius plots of ionic conductivities for cooling (—) and heating (- - -) scans of: a) NaTFSI(PEO)₉ and NaTFSI(PEO)₉ - Pyr₁₃TFSI and b) NaFSI(PEO)₉ and NaFSI(PEO)₉ - Pyr₁₃FSI. Lines are a guide to the eye only. Reproduced from V.

6 Conclusions and outlook

Every SIB electrolyte has its pro and cons. Organic liquid electrolytes, while guarantee a larger battery operating voltage than aqueous based electrolytes, suffer from severe safety concerns. A first step toward safer SIBs battery electrolytes is to use fluorine-free salts. A first generation of pseudo-localized anion based salts, while representing an appealing fix, suffers from low solubility in conventional organic solvents. Another approach toward safer electrolytes is to replace the organic liquid electrolyte with a solid polymer electrolyte (SPE). However, the SPEs suffer from low ion conduction, which hinder their utilization at room temperature. The conductivity could be further improved with addition of ionic liquids but their required amount is quite substantial (~50 wt%). In order to further improve the performance and the characterization of liquid and solids electrolytes the following suggestions are given:

- Aiming to fluorine-free salts, the synthesis of a second generation of MM anions, perhaps with shorter alkyl chain that could avoid the wrapping of the butyl sulfonate groups around the Na^+ , could lead to salts soluble in organic solvents.
- The dynamics of SPE could be improved using new kind of pseudo-localized ions which could reduce the interaction between ions and also act plasticizing.
- The concept of a solid state battery operating at RT could be viable adopting other electrolyte concepts. Single ion conductors, in which the ion conductivity is in principle carried solely by Na^+ , or polymers in which the conduction mechanism is decoupled from the polymer relaxation dynamics are two possible routes.
- The reliability of electrochemical characterization of SIB materials could be further improved by exploring suitable reference electrodes as *e.g.* sodium based alloys.

Acknowledgements

Time flies and I am about to finish my PhD. First of all I would like to thank my supervisor Patrik for giving me the opportunity to do a PhD at Chalmers. This work would have not been possible without the support from FORMAS, Energimyndigheten and the H2020 NAIADES project. Moreover Ångpanneföreningens forskningsstiftelse, Adlerbertska forskningsstiftelsen and Chalmersska forskningsfonden are acknowledged for travel grants.

Thank you to the past and present KMF members for the very nice environment, the discussions and company in the lab. I am really grateful to the colleagues that kindly gave me feedback about this thesis. Especially, I thank Manfred with whom I also shared teaching duties. Thanks to Carin and Martin with whom I have shared the office most of my time at KMF. All things in the lab could not run smoothly without Ezio, so a big thank you definitely goes to him. I would also like to thank the past and present members of the “extended” electrochemistry group at GU for discussions, lunches, and especially Kristoffer and Adriano, with whom I participated in a couple of conferences. Moreover, I would like to thank all the friends I met during these years in Göteborg and among them I mention Pippo & Laura.

A special mention goes to my family (especially to my brother Enrico) for the continuous support and encouragement: Grazie!

Duri i banchi!!

Andrea

Bibliography

- [1] N. Omar, M. Daowd, P. van den Bossche, O. Hegazy, J. Smekens, T. Coosemans, J. van Mierlo, *Energies* 5 (2012) 2952.
- [2] A. Yoshino, *Angew. Chemie Int. Ed.* 51 (2012) 5798.
- [3] C.-X. Zu, H. Li, *Energy Environ. Sci.* 4 (2011) 2614.
- [4] P.J. Hall, E.J. Bain, *Energy Policy* 36 (2008) 4352.
- [5] J.-M. Tarascon, *Nat. Chem.* 2 (2010) 510.
- [6] H. Vikström, S. Davidsson, M. Höök, *Appl. Energy* 110 (2013) 252.
- [7] A. Ponrouch, R. Dedryvère, D. Monti, A.E. Demet, J.M. Ateba Mba, L. Croguennec, C. Masquelier, P. Johansson, M.R. Palacín, *Energy Environ. Sci.* 6 (2013) 2361.
- [8] Q. Wang, P. Ping, X. Zhao, G. Chu, J. Sun, C. Chen, *J. Power Sources* 208 (2012) 210.
- [9] P.G. Balakrishnan, R. Ramesh, T.P. Kumar, *J. Power Sources* 155 (2006) 401.
- [10] Z. Chen, Y. Qin, Y. Ren, W. Lu, C. Orendorff, E.P. Roth, K. Amine, *Energy Environ. Sci.* 4 (2011) 4023.
- [11] G.G. Eshetu, S. Grugeon, S. Laruelle, S. Boyanov, A. Lecocq, J.-P. Bertrand, G. Marlair, *Phys. Chem. Chem. Phys.* 15 (2013) 9145.
- [12] J.F. Whitacre, T. Wiley, S. Shanbhag, Y. Wenzhuo, A. Mohamed, S.E. Chun, E. Weber, D. Blackwood, E. Lynch-Bell, J. Gulakowski, C. Smith, D. Humphreys, *J. Power Sources* 213 (2012) 255.
- [13] <http://aquionenergy.com> (accessed 2016-12-12).
- [14] <http://www.bluecar.fr> (accessed 2016-12-12) .
- [15] A. Matic, B. Scrosati, *MRS Bull.* 38 (2013) 533.
- [16] J.-H. Shin, W.A. Henderson, S. Passerini, *Electrochem. Commun.* 5 (2003) 1016.
- [17] J.-H. Shin, W.A. Henderson, S. Passerini, *J. Electrochem. Soc.* 152 (2005) A978.
- [18] A. Lewandowski, A. Świdarska-Mocek, *J. Power Sources* 194 (2009) 601.
- [19] D.M. Fox, J.W. Gilman, A.B. Morgan, J.R. Shields, P.H. Maupin, R.E. Lyon, H.C. De Long, P.C. Trulove, *Ind. Eng. Chem. Res.* 47 (2008) 6327.
- [20] B. Scrosati, *J. Solid State Electrochem.* 15 (2011) 1623.
- [21] A. Volta, *Philos. Trans. R. Soc. London* 90 (1800) 403.
- [22] V. Matovic, A. Buha, D. Dukic-Cosic, Z. Bulat, *Food Chem. Toxicol.* 78 (2015) 130.
- [23] W. Zhang, J. Yang, X. Wu, Y. Hu, W. Yu, J. Wang, J. Dong, M. Li, S. Liang, J. Hu, R.V. Kumar, *Renew. Sustain. Energy Rev.* 61 (2016) 108.
- [24] C. Daniel, J.O. Besenhard, *Handbook of Battery Materials*, Wiley, 2013.
- [25] <http://www.energizer.com> (accessed 2016-12-12).
- [26] R.J. Brodd, *Batteries for Sustainability: Selected Entries from the Encyclopedia of Sustainability Science and Technology*, Springer New York, 2012.
- [27] <http://www.peve.jp/en/index.html> (accessed 2016-12-12).
- [28] N. Nitta, F. Wu, J.T. Lee, G. Yushin, *Mater. Today* 18 (2015) 252.

- [29] A. Yoshino, in: G. Pistoia (Ed.), *Lithium-Ion Batter.*, Elsevier, Amsterdam, 2014, 1.
- [30] K.B. Hueso, M. Armand, T. Rojo, *Energy Environ. Sci.* 6 (2013) 734.
- [31] C.-H. Dustmann, *J. Power Sources* 127 (2004) 85.
- [32] Claus Daniel, J.O. Besenhard Jürgen, eds., *Handbook of Battery Materials*, 2nd ed., Wiley-VCH Verlag GmbH & Co, 2011.
- [33] M.S. Whittingham, *Prog. Solid State Chem.* 12 (1978) 41.
- [34] C. Delmas, J. Braconnier, C. Fouassier, P. Hagenmuller, *Solid State Ionics* 3–4 (1981) 165.
- [35] V. Palomares, P. Serras, I. Villaluenga, K.B. Hueso, J. Carretero-González, T. Rojo, *Energy Environ. Sci.* 5 (2012) 5884.
- [36] <http://www2.cnrs.fr/en/2659.htm> (accessed 2016-12-12).
- [37] A. Ponrouch, A.R. Goni, M. Rosa Palacin, *Electrochem. Commun.* 27 (2013) 85.
- [38] P. Thomas, D. Billaud, *Electrochim. Acta* 47 (2002) 3303.
- [39] Y. Wen, K. He, Y. Zhu, F. Han, Y. Xu, I. Matsuda, Y. Ishii, J. Cumings, C. Wang, *Nat. Commun.* 5 (2014).
- [40] P. Senguttuvan, G. Rouse, V. Seznec, J.-M. Tarascon, M. Rosa Palacin, *Chem. Mater.* 23 (2011) 4109.
- [41] S.-W. Kim, D.-H. Seo, X. Ma, G. Ceder, K. Kang, *Adv. Energy Mater.* 2 (2012) 710.
- [42] F. Klein, B. Jache, A. Bhide, P. Adelhelm, *Phys. Chem. Chem. Phys.* 15 (2013) 15876.
- [43] Z. Li, J. Ding, D. Mitlin, *Acc. Chem. Res.* 48 (2015) 1657.
- [44] W. Luo, F. Shen, C. Bommier, H. Zhu, X. Ji, L. Hu, *Acc. Chem. Res.* 49 (2016) 231.
- [45] S. Il Park, I. Gocheva, S. Okada, J. Yamaki, *J. Electrochem. Soc.* 158 (2011) A1067.
- [46] K. Kubota, I. Ikeuchi, T. Nakayama, C. Takei, N. Yabuuchi, H. Shiiba, M. Nakayama, S. Komaba, *J. Phys. Chem. C* 119 (2015) 166.
- [47] D. Hamani, M. Ati, J.-M. Tarascon, P. Rozier, *Electrochem. Commun.* 13 (2011) 938.
- [48] J. Billaud, R.J. Clément, A.R. Armstrong, J. Canales-Vázquez, P. Rozier, C.P. Grey, P.G. Bruce, *J. Am. Chem. Soc.* 136 (2014) 17243.
- [49] J.F. Whitacre, A. Tevar, S. Sharma, *Electrochem. Commun.* 12 (2010) 463.
- [50] X. Li, D. Wu, Y.-N. Zhou, L. Liu, X.-Q. Yang, G. Ceder, *Electrochem. Commun.* 49 (2014) 51.
- [51] K. Kubota, N. Yabuuchi, H. Yoshida, M. Dahbi, S. Komaba, *MRS Bull.* 39 (2014) 416.
- [52] C. Masquelier, L. Croguennec, *Chem. Rev.* 113 (2013) 6552.
- [53] D.B. Porter, R. Olazcuaga, C. Delmas, F. Cherkaoui, R. Brochu, G. Leflem, *Rev. Chim. Miner.* 17 (1980) 458.
- [54] Z. Jian, L. Zhao, H. Pan, Y.-S. Hu, H. Li, W. Chen, L. Chen, *Electrochem. Commun.* 14 (2012) 86.
- [55] R.A. Shakoor, D.-H. Seo, H. Kim, Y.-U. Park, J. Kim, S.-W. Kim, H. Gwon, S. Lee, K. Kang, *J. Mater. Chem.* 22 (2012) 20535.
- [56] R.J. Brodd, W.W. Huang, J.R. Akridge, *Macromol. Symp.* 159 (2000) 229.

- [57] A. Bhide, J. Hofmann, A. Katharina Dürr, J. Janek, P. Adelhelm, *Phys. Chem. Chem. Phys.* 16 (2014) 1987.
- [58] D. Monti, A. Ponrouch, M.R. Palacín, P. Johansson, *J. Power Sources* 324 (2016) 712.
- [59] X. Qi, Q. Ma, L. Liu, Y.-S. Hu, H. Li, Z. Zhou, X. Huang, L. Chen, *ChemElectroChem* 3 (2016) 1.
- [60] A. Hayashi, K. Noi, A. Sakuda, M. Tatsumisago, *Nat. Commun.* 3 (2012).
- [61] E. Peled, *J. Electrochem. Soc.* 126 (1979) 2047.
- [62] E. Peled, D. Golodnitsky, G. Ardel, V. Eshkenazy, *Electrochim. Acta* 40 (1995) 2197.
- [63] C. Xu, B. Sun, T. Gustafsson, K. Edström, D. Brandell, M. Hahlin, *J. Mater. Chem. A* 2 (2014) 7256.
- [64] D. Aurbach, B. Markovsky, M.D. Levi, E. Levi, A. Schechter, M. Moshkovich, Y. Cohen, *J. Power Sources* 81 (1999) 95.
- [65] K. Edström, T. Gustafsson, J.O. Thomas, *Electrochim. Acta* 50 (2004) 397.
- [66] P. Arora, Z.M. Zhang, *Chem. Rev.* 104 (2004) 4419.
- [67] H. Lee, M. Yanilmaz, O. Toprakci, K. Fu, X. Zhang, *Energy Environ. Sci.* 7 (2014) 3857.
- [68] H. Kim, J. Hong, K.-Y. Park, H. Kim, S.-W. Kim, K. Kang, *Chem. Rev.* 114 (2014) 11788.
- [69] A. Ponrouch, E. Marchante, M. Courty, J.-M. Tarascon, M.R. Palacín, *Energy Environ. Sci.* 5 (2012) 8572.
- [70] S. Komaba, W. Murata, T. Ishikawa, N. Yabuuchi, T. Ozeki, T. Nakayama, A. Ogata, K. Gotoh, K. Fujiwara, *Adv. Funct. Mater.* 21 (2011) 3859.
- [71] Z.W. Seh, J. Sun, Y. Sun, Y. Cui, *ACS Cent. Sci.* 1 (2015) 449.
- [72] A. Plewa-Marczewska, T. Trzeciak, A. Bitner, L. Niedzicki, M. Dranka, G.Z. Zukowska, M. Marcinek, W. Wieczorek, *Chem. Mater.* 26 (2014) 4908.
- [73] J. Foropolous, D.D. DesMarteau, *Inorg. Chem.* 23 (1984) 3720.
- [74] M. Armand, W. Gorecki, R. Andreani, in: *Proc. 2nd Int. Symp. Polym. Electrolytes*, B. Scrosati (Ed.), Elsevier, London, 1989, 91.
- [75] A. Vallee, S. Besner, J. Prudhomme, *Electrochim. Acta* 37 (1992) 1579.
- [76] M. Perrier, S. Besner, C. Paquette, A. Vallee, S. Lascaud, J. Prudhomme, *Electrochim. Acta* 40 (1995) 2123.
- [77] P. Johansson, S.P. Gejji, J. Tegenfeldt, J. Lindgren, *Electrochim. Acta* 43 (1998) 1375.
- [78] M. Kakihana, J. Sandahl, S. Schantz, L.M. Torell, in: *Proc. 2nd Int. Symp. Polym. Electrolytes*, B. Scrosati (Ed.), Elsevier, London, 1989, 1.
- [79] T. Caruso, S. Capoleoni, E. Cazzanelli, R.G. Agostino, P. Villano, S. Passerini, *Ionics* 8 (2002) 36.
- [80] L. Edman, *J. Phys. Chem. B* 104 (2000) 7254.
- [81] T.D. Hatchard, M.N. Obrovac, *J. Electrochem. Soc.* 161 (2014) A1748.
- [82] X. Xia, W.M. Lamanna, J.R. Dahn, *J. Electrochem. Soc.* 160 (2013) A607.
- [83] L. Suo, O. Borodin, T. Gao, M. Olguin, J. Ho, X. Fan, C. Luo, C. Wang, K. Xu, *Science* (80-.). 350 (2015) 938.

- [84] E. Jónsson, P. Johansson, *Phys. Chem. Chem. Phys.* 14 (2012) 10774.
- [85] H. Pan, X. Lu, X. Yu, Y.-S. Hu, H. Li, X.-Q. Yang, L. Chen, *Adv. Energy Mater.* 3 (2013) 1186.
- [86] G.G. Eshetu, S. Grugeon, H. Kim, S. Jeong, L. Wu, G. Gachot, S. Laruelle, M. Armand, S. Passerini, *ChemSusChem* 9 (2016) 462.
- [87] L. Otaegui, E. Goikolea, F. Aguesse, M. Armand, T. Rojo, G. Singh, *J. Power Sources* 297 (2015) 168.
- [88] Y.F. Chen, T.M. Devine, J.W. Evans, O.R. Monteiro, I.G. Brown, *J. Electrochem. Soc.* 146 (1999) 1310.
- [89] A. Abouimrane, J. Ding, I.J. Davidson, *J. Power Sources* 189 (2009) 693.
- [90] H.-B. Han, S.-S. Zhou, D.-J. Zhang, S.-W. Feng, L.-F. Li, K. Liu, W.-F. Feng, J. Nie, H. Li, X.-J. Huang, M. Armand, Z.-B. Zhou, *J. Power Sources* 196 (2011) 3623.
- [91] M. Kerner, N. Plylahan, J. Scheers, P. Johansson, *RSC Adv.* 6 (2016) 23327.
- [92] L. Korson, W. Drost-Hansen, F.J. Millero, *J. Phys. Chem.* 73 (1969) 34.
- [93] M. Pourbaix, *Atlas of Electrochemical Equilibria in Aqueous Solutions*, National Association of Corrosion Engineers, 1974.
- [94] J.F. Whitacre, S. Shanbhag, A. Mohamed, A. Polonsky, K. Carlisle, J. Gulakowski, W. Wu, C. Smith, L. Cooney, D. Blackwood, J.C. Dandrea, C. Truchot, *Energy Technol.* 3 (2015) 20.
- [95] M. Pasta, C.D. Wessells, N. Liu, J. Nelson, M.T. McDowell, R.A. Huggins, M.F. Toney, Y. Cui, *Nat. Commun.* 5 (2014).
- [96] E. Jónsson, M. Armand, P. Johansson, *Phys. Chem. Chem. Phys.* 14 (2012) 6021.
- [97] C. Wessells, R. Ruffo, R.A. Huggins, Y. Cui, *Electrochem. Solid-State Lett.* 13 (2010) A59.
- [98] D. Monti, E. Jónsson, M.R. Palacín, P. Johansson, *J. Power Sources* 245 (2014) 630.
- [99] C. Ding, T. Nohira, K. Kuroda, R. Hagiwara, A. Fukunaga, S. Sakai, K. Nitta, S. Inazawa, *J. Power Sources* 238 (2013) 296.
- [100] K.R. Seddon, *Nat. Mater.* 2 (2003) 363.
- [101] M. Joost, M. Kunze, S. Jeong, M. Schönhoff, M. Winter, S. Passerini, *Electrochim. Acta* 86 (2012) 330.
- [102] G. Yu, D. Zhao, L. Wen, S. Yang, X. Chen, *AIChE J.* 58 (2012) 2885.
- [103] J.B. Haskins, W.R. Bennett, J.J. Wu, D.M. Hernández, O. Borodin, J.D. Monk, C.W. Bauschlicher, J.W. Lawson, *J. Phys. Chem. B* 118 (2014) 11295.
- [104] S.A.M. Noor, P.C. Howlett, D.R. MacFarlane, M. Forsyth, *Electrochim. Acta* 114 (2013) 766.
- [105] T. Hosokawa, K. Matsumoto, T. Nohira, R. Hagiwara, A. Fukunaga, S. Sakai, K. Nitta, *J. Phys. Chem. C* 120 (2016) 9628.
- [106] D.R. MacFarlane, P. Meakin, J. Sun, N. Amini, M. Forsyth, *J. Phys. Chem. B* 103 (1999) 4164.
- [107] R.G. Pearson, *J. Am. Chem. Soc.* 85 (1963) 3533.
- [108] D.E. Fenton, J.M. Parker, P.V. Wright, *Polymer (Guildf)*. 14 (1973) 589.

- [109] M.B. Armand, J.M. Chabagno, M.J. Duclot, *Fast Ion Transp. Solids* (1979) 131.
- [110] K. West, B. Zachau-Christiansen, T. Jacobsen, S. Atlung, *J. Electrochem. Soc.* 132 (1985) 3061.
- [111] K. West, B. Zachau-Christiansen, T. Jacobsen, E. Hiort-Lorenzen, S. Skaarup, *Br. Polym. J.* 20 (1988) 243.
- [112] K. West, B. Zachau-Christiansen, T. Jacobsen, S. Skaarup, *J. Power Sources* 26 (1989) 341.
- [113] C.P. Rhodes, R. Frech, *Solid State Ionics* 121 (1999) 91.
- [114] S. Schantz, J. Sandhal, L. Börjesson, L.M. Torell, L.R. Stevens, *Solid State Ionics* 28–30 (1988) 1047.
- [115] A. Ferry, M.M. Doeff, L.C. De Jonghe, *J. Electrochem. Soc.* 145 (1998) 1586.
- [116] P.G. de Gennes, *J. Chem. Phys.* 55 (1971) 572.
- [117] J.E. Mark, *Physical Properties of Polymers Handbook*, Springer New York, 2007.
- [118] D. Golodnitsky, E. Strauss, E. Peled, S. Greenbaum, *J. Electrochem. Soc.* 162 (2015) A2551.
- [119] M.S.M. Alger, *Polymer Science Dictionary*, 1st Ed., 1990.
- [120] D.F. Cadogan and C.J. Howick, in: *Ullmann's Encycl. Ind. Chem.*, John Wiley & Sons Inc, 2012, p. 599.
- [121] L.R.A.K. Bandara, M.A.K.L. Dissanayake, M. Furlani, B.-E. Mellander, *Ionics* 6 (2000) 239.
- [122] M. Patel, K.G. Chandrappa, A.J. Bhattacharyya, *Solid State Ionics* 181 (2010) 844.
- [123] L.-Z. Fan, J. Maier, *Electrochem. Commun.* 8 (2006) 1753.
- [124] A.M. Stephan, *Eur. Polym. J.* 42 (2006) 21.
- [125] H. Gao, B. Guo, J. Song, K. Park, J.B. Goodenough, *Adv. Energy Mater.* 5 (2015) 1402235.
- [126] H. Gao, W. Zhou, K. Park, J.B. Goodenough, *Adv. Energy Mater.* 6 (2016) 1600467.
- [127] Y.Q. Yang, Z. Chang, M.X. Li, X.W. Wang, Y.P. Wu, *Solid State Ionics* 269 (2015) 1.
- [128] M.A. McArthur, S. Trussler, J.R. Dahn, *J. Electrochem. Soc.* 159 (2012) A198.
- [129] G.M. Veith, M. Doucet, J.K. Baldwin, R.L. Sacci, T.M. Fears, Y. Wang, J.F. Browning, *J. Phys. Chem. C* 119 (2015) 20339.
- [130] O. Borodin, G. V Zhuang, P.N. Ross, K. Xu, *J. Phys. Chem. C* 117 (2013) 7433.
- [131] S. Komaba, T. Ishikawa, N. Yabuuchi, W. Murata, A. Ito, Y. Ohsawa, *ACS Appl. Mater. Interfaces* 3 (2011) 4165.
- [132] J.B. Goodenough, Y. Kim, *Chem. Mater.* 22 (2010) 587.
- [133] M. Moshkovich, Y. Gofer, D. Aurbach, *J. Electrochem. Soc.* 148 (2001) E155.
- [134] A. Ponrouch, A.R. Goñi, M.R. Palacín, *Electrochem. Commun.* 27 (2013) 85.
- [135] N. Weadock, N. Varongchayakul, J.Y. Wan, S. Lee, J. Seog, L.B. Hu, *Nano Energy* 2 (2013) 713.
- [136] D.I. Iermakova, R. Dugas, M.R. Palacín, A. Ponrouch, *J. Electrochem. Soc.* 162 (2015) A7060.

- [137] P.G. Bruce, C.A. Vincent, *J. Chem. Soc. Faraday Trans.* 89 (1993) 3187.
- [138] C. Sequeira, D. Santos, *Polymer Electrolytes: Fundamentals and Applications*, Elsevier Science, 2010.
- [139] N.A. Stolwijk, M. Wiencierz, S. Obeidi, *Faraday Discuss.* 134 (2007) 157.
- [140] N.A. Stolwijk, M. Wiencierz, S. Obeidi, *Electrochim. Acta* 53 (2007) 1575.
- [141] M.J. Hudson, C.A.C. Sequeira, *J. Electrochem. Soc.* 142 (1995) 4013.
- [142] S. Zugmann, M. Fleischmann, M. Amereller, R.M. Gschwind, H.D. Wiemhofer, H.J. Gores, *Electrochim. Acta* 56 (2011) 3926.
- [143] J. Evans, C.A. Vincent, P.G. Bruce, *Polymer* 28 (1987) 2324.
- [144] Y. Ma, M. Doyle, T.F. Fuller, M.M. Doeff, L.C. De Jonghe, J. Newman, *J.E. Soc., L.C. Jonghe*, (1995).
- [145] M.A. Estes, M.L. Llorente, *J. Chem. Eng. Data* 28 (1983) 337.
- [146] H. Vogel, *Phys. Zeitschrift* 22 (1921) 645.
- [147] G. Tammann, W. Hesse, *Zeitschrift Für Anorg. Und Allg. Chemie* 156 (1926).
- [148] G.S. Fulcher, *J. Am. Ceram. Soc.* 8 (1925) 339.
- [149] M. Armand, J.M. Chabagno, M.J. Duclot, in: P. Vashista, J.N. Mundy, G.K. Shenoy (Eds.), North-Holland, Amsterdam, 1979, 131.
- [150] M.H. Cohen, D. Turnbull, *J. Chem. Phys.* 31 (1959) 1164.
- [151] J.H. Gibbs, E.A. DiMarzio, *J. Chem. Phys.* 28 (1958) 373.
- [152] E. Staunton, Y.G. Andreev, P.G. Bruce, *Faraday Discuss.* 134 (2007) 143.
- [153] C.H. Zhang, S. Gamble, D. Ainsworth, A.M.Z. Slawin, Y.G. Andreev, P.G. Bruce, *Nat. Mater.* 8 (2009) 580.
- [154] O. Borodin, G.D. Smith, *J. Solution Chem.* 36 (2007) 803.
- [155] O. Borodin, G.D. Smith, W. Henderson, *J. Phys. Chem. B* 110 (2006) 16879.
- [156] D. Devaux, R. Bouchet, D. Glé, R. Denoyel, *Solid State Ionics* 227 (2012) 119.
- [157] O. Borodin, G.D. Smith, *Macromolecules* 39 (2006) 1620.
- [158] M.A. Ratner, D.F. Shriver, *Chem. Rev.* 88 (1988) 109.
- [159] O. Dürr, *Solid State Ionics* 149 (2002) 125.
- [160] Y. Wang, F. Fan, A.L. Agapov, T. Saito, J. Yang, X. Yu, K. Hong, J. Mays, A.P. Sokolov, *Polymer* 55 (2014) 4067.
- [161] Y. Wang, A.P. Sokolov, *Curr. Opin. Chem. Eng.* 7 (2015) 113.
- [162] A.L. Agapov, A.P. Sokolov, *Macromolecules* 44 (2011) 4410.
- [163] S.K. Fullerton-Shirey, L.V.N.R. Ganapatibhotla, W. Shi, J.K. Maranas, *J. Polym. Sci. Part B Polym. Phys.* 49 (2011) 1496.
- [164] H. Gao, J.B. Goodenough, *Angew. Chemie Int. Ed.* 55 (2016) 12768.
- [165] Y. Yamada, A. Yamada, *J. Electrochem. Soc.* 162 (2015) A2406.
- [166] J. Wang, Y. Yamada, K. Sodeyama, C.H. Chiang, Y. Tateyama, A. Yamada, *Nat. Commun.* 7 (2016) 12032.
- [167] Y. Yamada, M. Yaegashi, T. Abe, A. Yamada, *Chem. Commun.* 49 (2013) 11194.

- [168] K. Matsumoto, K. Inoue, K. Nakahara, R. Yuge, T. Noguchi, K. Utsugi, J. Power Sources 231 (2013) 234.
- [169] F.M. Gray, Solid Polymer Electrolytes: Fundamentals and Technological Applications, Wiley-VCH, 1991.
- [170] M. Volel, M. Armand, W. Gorecki, Macromolecules 37 (2004) 8373.
- [171] G.B. Appetecchi, Y. Aihara, B. Scrosati, Solid State Ionics 170 (2004) 63.
- [172] F. Gray, J. Maccallum, C. Vincent, Solid State Ionics 18–19 (1986) 282.
- [173] J.-H. Shin, F. Alessandrini, S. Passerini, J. Electrochem. Soc. 152 (2005) A283.
- [174] J.-H. Shin, W.A. Henderson, C. Tizzani, S. Passerini, S.-S. Jeong, K.-W. Kim, J. Electrochem. Soc. 153 (2006) A1649.
- [175] M. Wetjen, G.-T. Kim, M. Joost, G.B. Appetecchi, M. Winter, S. Passerini, J. Power Sources 246 (2014) 846.
- [176] B. Rupp, M. Schmuck, A. Balducci, M. Winter, W. Kern, Eur. Polym. J. 44 (2008) 2986.
- [177] W.F. Höhne, W.F. Hemminger, H.-J. Flammersheim, Differential Scanning Calorimetry, 2003, Springer-Verlag Berlin Heidelberg GmbH, Berlin, 2003.
- [178] <http://www.tainstruments.com> (accessed 2016-12-12).
- [179] P.J. Haines, Principles of Thermal Analysis and Calorimetry, Royal Society of Chemistry, 2002.
- [180] A. Fadini, F.M. Schnepel, Vibrational Spectroscopy: Methods and Applications, E. Horwood, 1989.
- [181] P. Larkin, Infrared and Raman Spectroscopy: Principles and Spectral Interpretation, Elsevier Science, 2011.
- [182] R.J. Meier, Vib. Spectrosc. 39 (2005) 266.
- [183] I. Rey, P. Johansson, J. Lindgren, J.C. Lassègues, J. Grondin, L. Servant, J. Phys. Chem. A 102 (1998) 3249.
- [184] B.L. Papke, M.A. Ratner, D.F. Shriver, J. Phys. Chem. Solids 42 (1981) 493.
- [185] C.P. Rhodes, R. Frech, Macromolecules 34 (2001) 2660.
- [186] B. Schrader, Infrared and Raman Spectroscopy: Methods and Applications, Wiley, 2008.
- [187] D. Guyomard, J.M. Tarascon, J. Electrochem. Soc. 139 (1992) 937.
- [188] M.E. Orazem, B. Tribollet, Electrochemical Impedance Spectroscopy, Wiley, 2011.
- [189] A. Lasia, Electrochemical Impedance Spectroscopy and Its Applications, Springer New York, 2014.
- [190] E. Barsoukov, J.R. Macdonald, Impedance Spectroscopy: Theory, Experiment, and Applications, Wiley, 2005.
- [191] http://www.novocontrol.de/html/index_analyzer.htm (accessed 2016-12-12).
- [192] F. Kremer, A. Schönhals, Broadband Dielectric Spectroscopy, Springer Berlin Heidelberg, 2002.
- [193] J.R. MacCallum, C.A. Vincent, Polymer Electrolyte Reviews, Elsevier Applied Science, 1987.

- [194] T. Pajkossy, *J. Electroanal. Chem.* 364 (1994) 111.
- [195] S.K. MacLeod, *Anal. Chem.* 63 (1991) 557A.
- [196] W. Fischer, *Anal. Chim. Acta* 257 (1992) 165.
- [197] K. Fischer, *Angew. Chemie* 48 (1935) 394.
- [198] <http://www.metrohm.com> (accessed 2016-12-12).
- [199] C.M.A. Brett, A.M.O. Brett, *Electrochemistry: Principles, Methods, and Applications*, Oxford University Press, 1993.